M. Tech. Power Electronics & Systems

Prajeet Shukla

2022

Investigation on

LLC resonant converter transient handling

A DISSERTATION

SUBMITTED IN PARTIAL FULFILLMENT OF THE REQUIREMENTS

FOR THE AWARD OF THE DEGREE

OF

MASTER OF TECHNOLOGY

IN

POWER ELECTRONICS AND SYSTEMS

Submitted by:

PRAJEET SHUKLA

2K20/PES/13

Under the supervision of

Prof. Vishal Verma

DEPARTMENT OF ELECTRICAL ENGINEERING

DELHI TECHNOLOGICAL UNIVERSITY

(Formerly Delhi College of Engineering)

Bawana Road, Delhi-110042

JUNE, 2022

DEPARTMENT OF ELECTRICAL ENGINEERING

DELHI TECHNOLOGICAL UNIVERSITY

(Formerly Delhi College of Engineering)

Bawana Road, Delhi-110042

CANDIDATE'S DECLARATION

I, Prajeet Shukla, Roll No. 2K20/PES/13 student of MTech (Power Electronics and Systems), hereby declare that the project Dissertation titled "**Investigation on LLC resonant converter transient handling**" which is submitted by me to the Department of Electrical Engineering, Delhi Technological university, Delhi in partial fulfilment of the requirement for the award of the degree of Master of Technology, is original and not copied from any source without proper citation. This work has not previously formed the basis for the award of any Degree, Diploma Associateship, Fellowship or other similar title or recognition.

Place: Delhi — Prajeet Shukla

Date: 31 May 2022 — (2K20/PES/13)

DEPARTMENT OF ELECTRICAL ENGINEERING

DELHI TECHNOLOGICAL UNIVERSITY

(Formerly Delhi College of Engineering)

Bawana Road, Delhi-110042

CERTIFICATE

I hereby certify that the project Dissertation titled "**Investigation on LLC resonant converter transient handling**" which is submitted by Prajeet Shukla, Roll No. 2K20/PES/13, Department of Electrical Engineering, Delhi Technological University, Delhi in partial fulfilment of the requirement for the award of the degree of Master of Technology, is a record of the project work carried out by the students under my supervision. To the best of my knowledge this work has not been submitted in part or full for any Degree or Diploma to this University or elsewhere.

Place: Delhi

Date: 31 May 2022

Supervisor

Dr. Vishal Verma

DEPARTMENT OF ELECTRICAL ENGINEERING

DELHI TECHNOLOGICAL UNIVERSITY

(Formerly Delhi College of Engineering)

Bawana Road, Delhi-110042

ACKNOWLEDGEMENT

I would like to express my gratitude towards all the people who have contributed their precious time and effort to help me without whom it would not have been possible for me to understand and complete the project.

I would like to thank Dr. Vishal Verma (Professor), DTU Delhi, Department of Electrical Engineering, my Project supervisor, for supporting, motivating and encouraging me throughout the period of this work was carried out. His readiness for consultation at all times, his educative comments, his concern and assistance even with practical things have been invaluable.

Date: 31/05/22

Prajeet Shukla
MTech (Power Electronics &Systems)
Roll No. 2K20/PES/13

ABSTRACT

In this thesis we introduce novel dual input common tank step-down high-power LLC resonant converter topology as well as standard LLC topology for DC distribution with on load start and dynamic load control features intact. Although, the proposed topology used in these converters can be used in range of applications, the operating voltage and power level used in this thesis is in according to off-grid DC energy solutions. The nominal 380V bus voltage is step down to 96V utilizing LLC resonant converter operating at 150kHz switching frequency and 3.3KW power level.

The first architecture is the conventional LLC topology. Using Variable frequency control, the tank impedance is controlled as per different load condition. The Proposed Converter discusses the control algorithm to suppress the inrush starting current of the resonant converter with fast dynamics. The Proposed converter is able to handle the inrush current by switching the converter at the start with twice the resonant frequency and reducing the switching frequency to near resonant frequency while at the steady state condition the variable switching frequency control is achieved using look up table method.

The second architecture introduces changes in the conventional LLC topology to source power from two Photovoltaic sources operating at differential mode for achieving even faster charging with dynamic control.

Both proposed architectures are suitable to handle starting transient current and load perturbations with fast dynamics.

Contents

LIST OF FIGURES

LIST OF TABLES

CHAPTER-1
INRODUCTION

1.1 BACKGROUND

Today's loads are changing rapidly as a result of semiconductor innovation and the progress of power electronic converter systems. Spacecraft, data centers, telecommunication, traction, and naval power systems all use DC distribution [1]. DC electricity is required for laptops, cell phones, televisions, microwave ovens, and energy-efficient lighting. Industrial loads, such as the steel industry, have begun to employ DC electric arc furnaces increasingly because they are more efficient than matching AC arc furnaces. Load and line regulation, transient handling, EMI suppression, energy savings, grid integration hurdles, and more are all issues that modern converter systems face while controlling electronic loads [1], [2] As a result of the nature of load demand, the requirement for increased efficiency, improved load control, and cost savings, transition to DC distribution has occurred across several sectors and applications. The current AC distribution system as shown in Fig.1.1, which includes multiple conversion stages, is inefficient. DC distribution system as shown in Fig.1.2, uses high-frequency power transfer which minimizes the size of filters and transformers and makes the system less bulky and cost effective [2]. Wide adoption of dc distribution is enabled by highly efficient converter systems that can drive the load over a wide input voltage and load range while running at high efficiency throughout the operation cycle. Even with a DC distribution system, the ability to integrate static energy storage devices like batteries and ultra-capacitors expands the system's capabilities [3]. The DC-DC converter is a critical interface for the effective installation of a DC distribution system because it delivers the necessary voltage level changes. LLC Resonant converter has become the usual choice with the advent of high frequency converter technology as it operates with low switching losses, utilizing sinusoidal flux coupling for efficient magnetic circuit operation and exhibits operation with wider input voltage range and load perturbations. However, control of LLC resounding converter is as yet complex to carry out as result is constrained by fast transient reaction of resonant tank. Out of many control techniques reported, frequency

control is the simpler and easy to implement for LLC converter as the resonant tank impedance can be directly controlled by switching frequency [4]. Also, the relationship between the control signal and frequency shows linear characteristics, which can alleviate the need of complex non-linear controllers. With variable frequency control, resonant tank continuously exchanges pulsating energy with the source resulting into circulating losses which becomes worst at light load conditions where system efficiency is most adversely affected. Burst mode control technique is frequently used to increase efficiency when dealing with light loads [4], [5]. Beside this, at staring the converter witness a large inrush current and voltage stresses on primary switches which may lead to permanent damage to the switches [5], [6]. Optimal trajectory control is presented in the literature to demonstrate effective operation, but due to involvement of complex mathematical expressions, duly aided by multiple sensors become tedious to implement on fixed point microcontrollers [7], [8]. In the literature [6], [7], average geometric control is explored, which is based on an average large signal model to forecast large signal behavior and, as a result, regulate transients with extensive calculations.

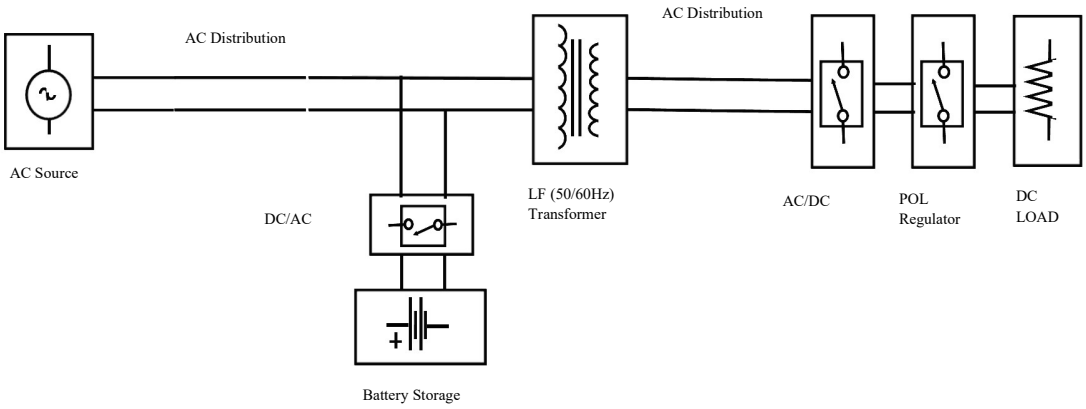

Fig 1.1 AC Distribution network

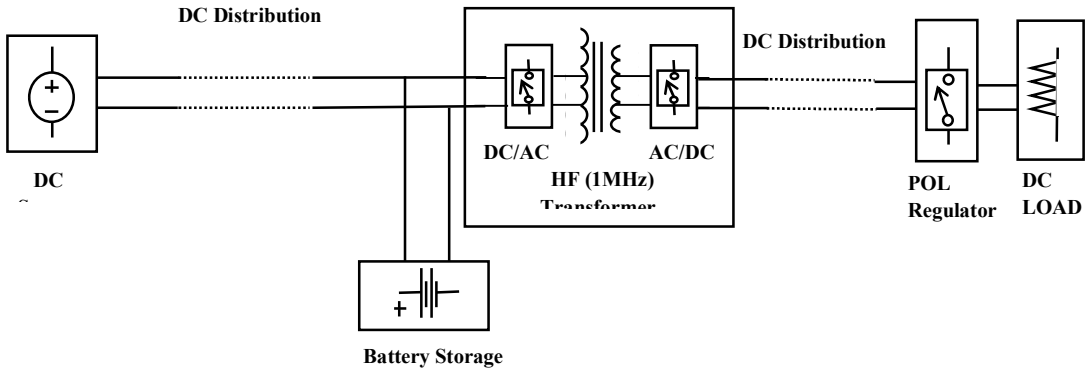

Fig.1.2 DC distribution network

1.2 THESIS OBJECTIVES

The work done in the thesis is primarily focused on providing cost effective and easy to implement control scheme for curtailing stating inrush current and to handle transients during dynamic load changes in large step-down LLC resonant converter for Dc distribution. Converter design and Magnetics design to handle large current of the order of 40A is also carried out in the study presented. Apart from control technique for handling transients in the conventional LLC topology, a novel PV based dual input common tank LLC topology is presented for Off grid charging application. The novel topology helps in achieving fast charging while other features of conventional LLC topology remaining intact.

1.3 THESIS ORGANIZATION

This proposal's work has been divided into seven sections. Chapter 1 briefs introduction. Chapter 2 discusses the conventional LLC topology, its features along with different modes of operation. The implementation of control in LLC resonant converters and various control mechanisms are discussed in Chapter 3. The LLC resonant converter component selection and magnetics design are demonstrated in Chapter 4. In Chapter 5, the transient handling using proposed control scheme is presented along with simulation results and performance analysis are discussed. In Chapter 6, Novel Dual input common tank resonant charger results are demonstrated using simulation results. With Conclusion and future work thesis is summarized in chapter 7.

CHAPTER-2
LLC RESONANT CONVERTER

2.1 Circuit Description

The LLC resonant converter circuit is shown in Fig 2.1, which consists of Class D inverter and center taped Class D rectifier. The resonant tank Cr-Lr-Lm is trapped between the legs of the H bridge inverter. The rectifier section is center tapped and load is connected in parallel to the output capacitive filter C_o. A high-frequency transformer, which is significantly smaller than a low-frequency transformer, can be put between the inverter and the rectifier if isolation is necessary. Switches SW_1, SW_4 and SW_2, SW_3 are alternately switched with a duty cycle of almost 50% under steady state operation, thereby handing over the command to variable frequency control for tweaking the impedance of resonant tank. DC voltage transfer function of LLC resonant converter which is almost insensitive to the load variations. In addition, the circuit has high efficiency over a wide range of load perturbations.

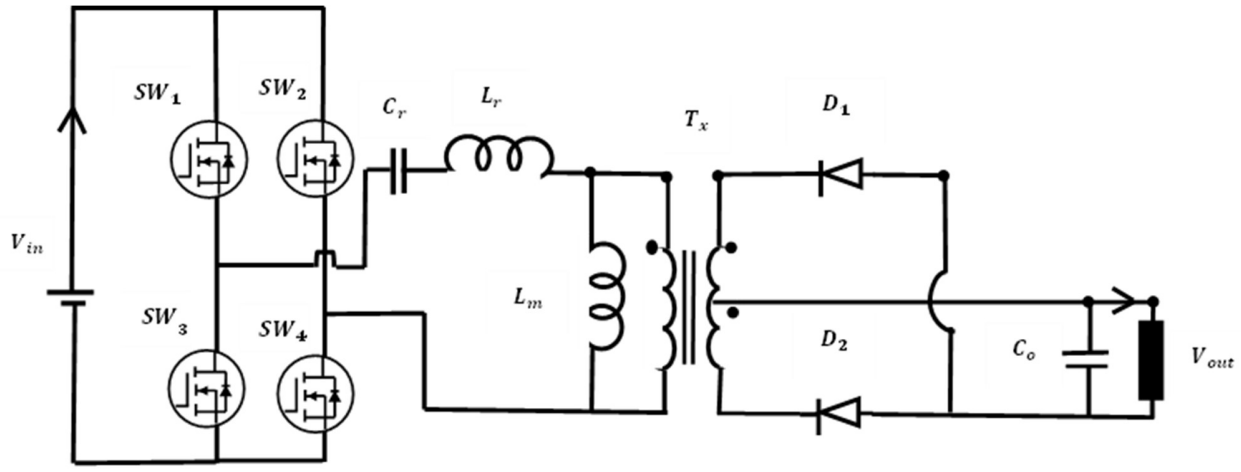

Fig.2. 1 Full Bridge LLC Resonant Converter

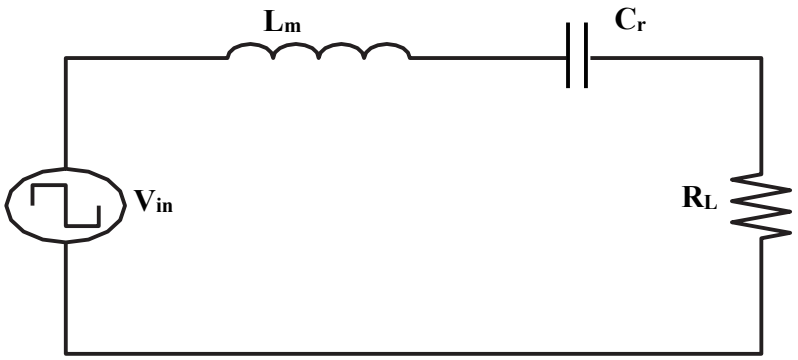

Fig.2. 2 Equivalent Circuit of Series Resonant Converter

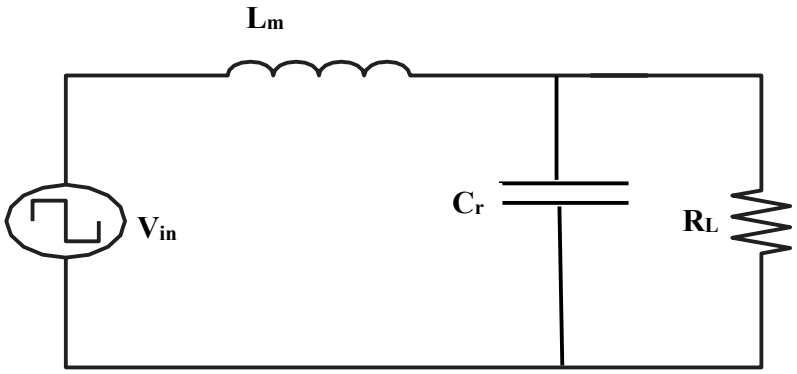

Fig.2. 3 Equivalent Circuit of Parallel Resonant Converter

Three well-known resonant topologies are series resonant, parallel resonant, and series-parallel resonant[9]– [12]. The basic operation of each of these topologies is the same: a square pulse of voltage or current is formed and applied to the resonant tank circuit. The energy that circulates inside the resonant tank is either fully transferred to the output load or dissipated inside the tank circuit. The series and parallel resonant topologies shown in Fig.2.2 and Fig.2.3 have major limitations, rendering them unsuitable for practical use. To maintain output voltage control during light load operation, the series resonant converter architecture requires a wide range of switching frequencies. Under high input voltage conditions, the series resonant converter suffers considerable conduction losses, and the switching network transistors encounter high turn-on current[9]. The Series Resonant Converter (SRC) is a type of LLC converter in which the magnetizing inductance is rather big and does not participate in the resonance operation.

Compared to a traditional series resonant converter, the LLC converter has numerous advantages. It may, for example, maintain very high efficiency while regulating output voltage over a large range of line and load fluctuations with a relatively modest change in switching frequency[13]. Over the whole operating range, it can also function at zero voltage switching (ZVS).

Fig.1 depicts a Full Bridge LLC converter with all parameters, including the magnetizing inductance, reflected to the primary side of the transformer.

Unlike the series resonant converter, the parallel resonant converter does not require a large range of switching frequencies to maintain output voltage control. When the input voltage is large, the parallel resonant converter, on the other hand, has worse conduction losses and higher turn-on currents[14].

The series-parallel or LCC (inductor-capacitor-capacitor) converter depicted in Figure 2.4 is one possible approach to mitigate the limitations found in the prior two converters[10], [15]. It is desired to operate the converter around the resonant frequency because it is known that this operating point has the highest efficiency.

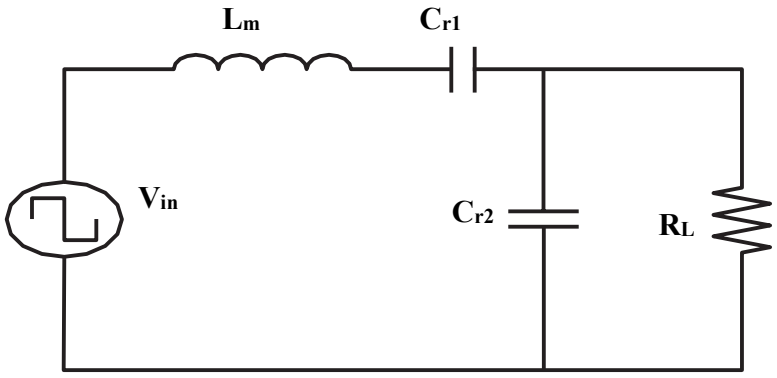

Fig.2. 4 Equivalent Circuit Diagram of Series Parallel (LCC) Resonant converter

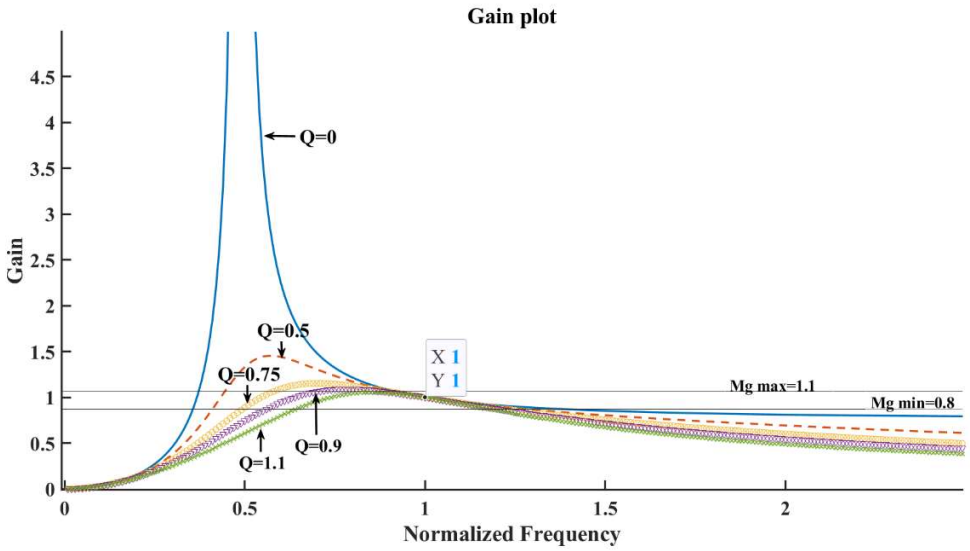

Fig.2. 5 DC Gain Characteristic of LLC resonant converter

The DC gain characteristic of the LLC resonant converter is shown in Fig.2.5 for various values of the variable Q, and it can be seen that there are multiple resonant frequencies depending on the value of Q.

Q, which is defined as the ratio between the characteristic impedance and the output load, may be calculated using Equation.

$$Q = \frac{\sqrt{L_r/C_r}}{R_e} \tag{2.1}$$

where, R_e, denotes the reflected output load resistance.

Furthermore, the areas of the DC gain characteristic with a positive gradient are suited for zero-current switching (ZCS) operation[13], [16]–[20]. The designed converter will use metal-oxide field-effect transistors (MOSFETs) as the semiconductor switching device for which the ideal operating area is on the negative gradient. This is because ZVS is the most used soft-switching technique in MOSFET devices. ZVS lowers switching loss caused by diode recovery charge and semiconductor capacitance, which are typical in MOSFET switching devices. Because operation on the negative gradient of the DC gain characteristic is necessary, the characteristics of this operating region should be investigated[21].

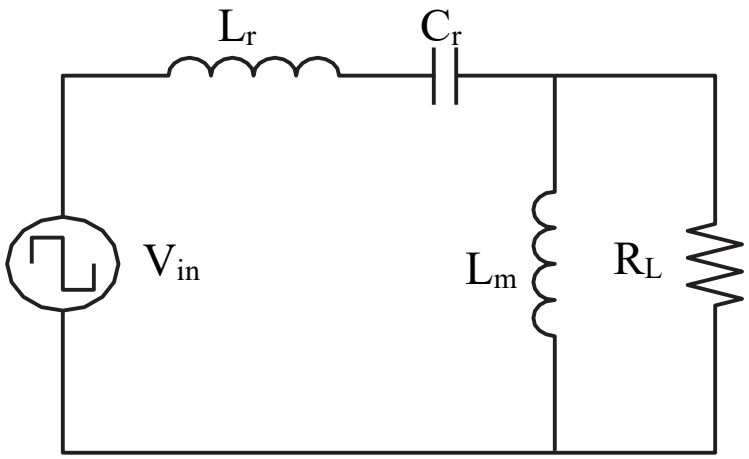

Fig.2. 6 Equivalent circuit of LLC Converter

2.2 Modes of Operation:

Mode I-

The primary switch S1 is turned on, and the secondary-side rectifier D2 receives the resonant current. In this mode, the output voltage clamps the magnetizing inductor L_m. The equivalent circuit is shown in Fig. 2.7, with the resonant capacitor Cr and the resonant inductor Lr forming the series resonant tank, and $V_{in} - nV_0$ being the source voltage across the resonant tank.

As a result, the current and voltage equations for the inductor and capacitor are:

$$\frac{dv_{cr}}{dt} = \frac{i_{Lr}}{C_r} \tag{2.2}$$

$$\frac{di_{Lr}}{dt} = -\frac{v_{cr}}{L_r} + \frac{1}{L_r}(V_{in} - nV_0) \tag{2.3}$$

where v_{cr} and i_{Lr} are the series resonant capacitor voltage and series resonant inductor current respectively.

Adding (2.2) and (2.3) we get,

$$v_{cr} - (V_{in} - nV_0) = I_{Lr0} Z_0 \sin[\omega_0(t - t_0)] + \left[V_{cr_0} - (V_{in} - nV_0)\right] \cos[\omega_0(t - t_0)] \tag{2.4}$$

$$i_{L_r} = I_{Lr_0}\cos[\omega_0(t-t_0)] - \frac{\left[V_{cr_0} - (V_{in} - nV_0)\right]}{Z_0}\sin[\omega_0(t-t_0)] \qquad (2.5)$$

where V_{cr_0} and I_{Lr0} are the initial series resonant capacitor voltage and series resonant inductor current at the time $t = t_0$, $\omega_0 = \frac{1}{\sqrt{L_r C_r}}$ is the resonant frequency, and $Z_0 = \sqrt{\frac{L_r}{C_r}}$ is the characteristic impedance.

The following equation is generated by normalizing all voltages with the voltage factor V_{in}, and all current factors with $\frac{V_{in}}{Z_0}$ in (2.4) and (2.5).

$$v_{Cr_N} - (1 - nV_{0N}) = I_{Lr0_n}\sin[\omega_0(t-t_0)] + \left[V_{Cr_{0N}} - (1 - nV_{0N})\right]\cos[\omega_0(t-t_0)] \qquad (2.6)$$

$$i_{L_{rN}} = I_{Lr_{0N}}\cos[\omega_0(t-t_0)] - \left[V_{Cr_{0N}} - (1 - nV_{0N})\right]\sin[\omega_0(t-t_0)] \qquad (2.7)$$

In equations (2.6) and (2.7), the subscript N stands for normalized circuit variables.
The trajectory equations for (2.6) and (2.7) are given by

$$\left[v_{Cr_N} - (1 - nV_{0N})\right]^2 + {i_{L_{rN}}}^2 = \left[V_{Cr_{0N}} - (1 - nV_{0N})\right]^2 + {I_{Lr_{0N}}}^2 \qquad (2.8)$$

Which behaves as a circle as shown in the fig.2.7 with a radius dictated by the beginning circumstances and I_{Lr_0} and V_{Cr_0}, a center determined by the source voltages $(1 - nV_{0N}, 0)$ across the tank.

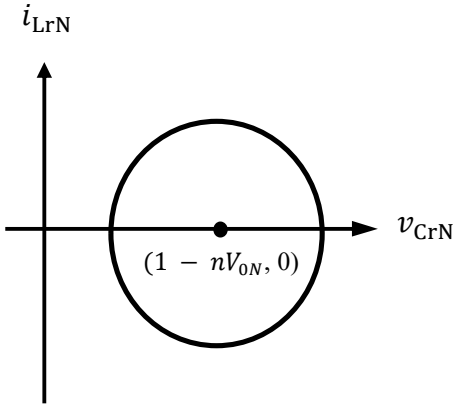

Fig.2. 7 State plane Trajectory of Mode I

Mode II-

When Switch S1 is turned on in Mode II, the current flowing through the secondary side reverses. It happens when the switching frequency f_s reaches the resonance frequency $f_0 = \frac{\omega_0}{2\pi}$. It is the same as mode I except $V_{in} + nV_0$, is the source voltage across the resonant tank.

Like Mode I, the trajectory expressions are given by

$$\left[v_{Cr_N} - (1 + nV_{0N})\right]^2 + {i_{L_{rN}}}^2 = \left[V_{Cr_{0N}} - (1 + nV_{0N})\right]^2 + {I_{Lr_{0N}}}^2 \qquad (2.9)$$

With the center altered to $(1 + nV_{0N}, 0)$, it operates similarly to a circle as shown in Fig.2,8.

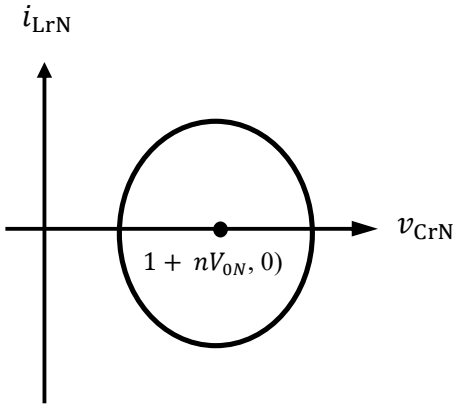

Fig.2. 8 State plane Trajectory of Mode II

Mode III-

When $f_s < f_0$, this mode appears, Switch S1 remains turned on in mode. Lm, the magnetizing inductance, joins the resonance in this mode and the secondary side current remains zero. Vin is the source voltage across the resonant tank and

$$\frac{dv_{cr}}{dt} = \frac{1}{L_r} i_{Lr} \qquad (2.10)$$

$$\frac{di_{Lr}}{dt} = -\frac{1}{(L_r + L_m)} v_{Cr} + \frac{1}{(L_r + L_m)} V_{in} \qquad (2.11)$$

From (2.10) and (2.11), v_{Cr} and i_{Lr} in mode III are given by

$$v_{Cr} - V_{in} = I_{Lr0} \cdot Z_1 \cdot \sin[\omega_1(t - t_0)] + (V_{Cr0} - V_{in}) \cdot \cos[\omega_1(t - t_0)] \qquad (2.12)$$

$$i_{L_r} = I_{Lr_0} \cos[\omega_1(t - t_0)] - \frac{\left[V_{cr_0} - (V_{in} - nV_0)\right]}{Z_1} \sin[\omega_1(t - t_0)] \qquad (2.13)$$

where $Z_1 = \sqrt{\frac{(L_r + L_m)}{C_r}}$ is the characteristic impedance, and $\omega_1 = \frac{1}{\sqrt{(L_r + L_m)C_r}}$ is the parallel resonant frequency when L_m participates in the resonance.

The normalized forms of v_{Cr} and i_{Lr} have the same normalising factors.

$$v_{CrN} - 1 = \frac{I_{Lr0N}}{Z_0/Z_1} \cdot \sin[\omega_1(t - t_0)] + (V_{Cr0N} - 1) \cdot \cos[\omega_1(t - t_0)] \qquad (2.14)$$

$$\frac{i_{L_rN}}{Z_0/Z_1} = \frac{I_{Lr_0}}{Z_0/Z_1} \cos[\omega_1(t - t_0)] - (V_{Cr0N} - 1) \cdot \sin[\omega_1(t - t_0)] \qquad (2.15)$$

The trajectory is obtained from (2.14) and (2.15)

$$\left(v_{Cr_N} - 1\right)^2 - \left(\frac{i_{L_rN}}{Z_0/Z_1}\right)^2 = \left[V_{Cr_{oN}} - 1\right]^2 + \left(\frac{I_{Lr0N}}{Z_0/Z_1}\right)^2 \qquad (2.16)$$

which is ellipse equation with center at (1,0). The characteristic impedance Z_1 becomes large ($Z_1 > Z_0$) as L_m participates in the resonance. The trajectory will be an ellipse if it is normalized with the same current factor V_{in}/Z_0.

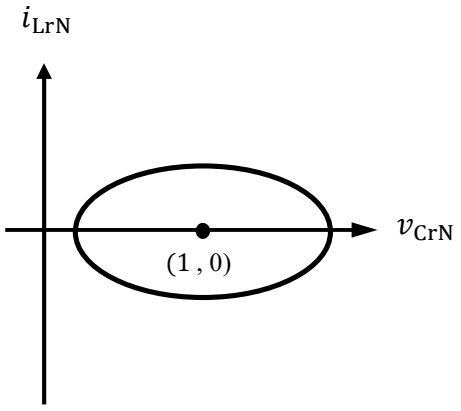

Fig.2. 9 State plane Trajectory of Mode III

There are three additional operation modes as illustrated in Fig. 3 if switch S_1 is turned off and switch S_2 is switched on.

Mode IV-

As shown in Fig. 3, switch S2 is turned on in this Mode, and the resonant current conducted through secondary-side rectifier diode D1. The only variation from Mode I is that the source voltage across the resonant tank changes to nV_o.

The state plane trajectory's normalized equation is:

$$\left[v_{Cr_N} - nV_{oN}\right]^2 + {i_{L_{rN}}}^2 = \left[V_{Cr_{oN}} - nV_{0N}\right]^2 + {I_{Lr_{oN}}}^2 \qquad (2.17)$$

as a result, the circle's center shifts to (nV_{oN}, 0) as shown in the Fig.2.10.

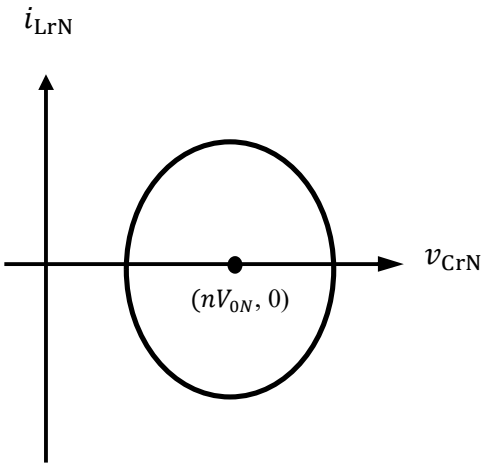

Fig.2. 10 State plane Trajectory of Mode IV

Mode V-

In Mode V, S_2 is turned on, but the current on the secondary side reverses and flows via rectifier Diode D2, as seen in Fig. 3. Similar, to Mode II this occurs when $f_s > f_0$. The trajectory's normalized expression is:

$$\left[v_{Cr_N} + nV_{0N}\right]^2 + {i_{L_rN}}^2 = \left[V_{Cr_{oN}} + nV_{0N}\right]^2 + {I_{Lr_{oN}}}^2 \qquad (2.18)$$

(nV_{0N}N, 0) is the circle's center.

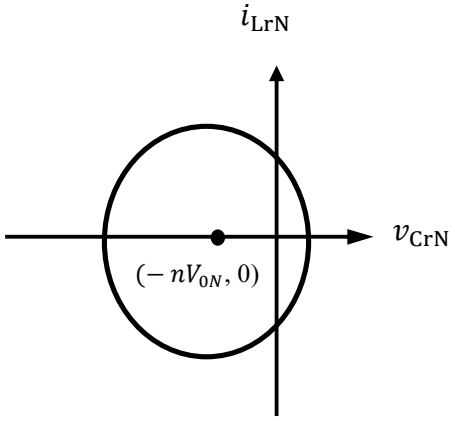

Fig.2. 11 State plane Trajectory of Mode V

Mode VI-

In Mode VI, S_2 is turned on, but no current flows through the secondary side. This mode appears with $f_s < f_0$. Cr, Lr, and Lm make up the series resonant tank, just as they do in Mode III. However, over the resonant tank, the source voltage drops to zero. Following normalization, the trajectory becomes

$$\left(v_{C_{rN}}\right)^2 - \left(\frac{i_{L_rN}}{Z_0/Z_1}\right)^2 = {V_{Cr_{0N}}}^2 + \left(\frac{I_{Lr0\mathrm{N}}}{Z_0/Z_1}\right)^2 \tag{2.19}$$

which is an ellipse with a center (0, 0).

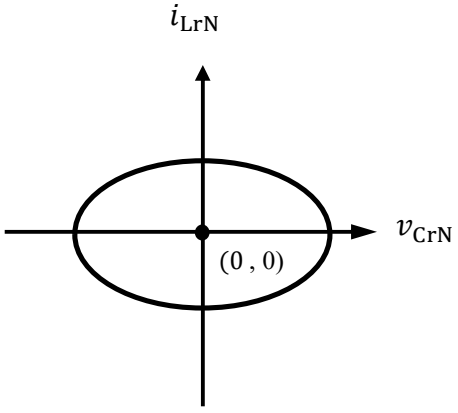

Fig.2. 12 State plane Trajectory of Mode VI

CHAPTER 3
CONTROL OF LLC RESONANT CONVERTER

3.1 INTRODUCTION

Switch mode converters are largely categorized into pulse width modulated (PWM) converters and resonant converters based on their circuit topologies and controls. The time constant of the output energy storage filter in a PWM converter is typically much larger than the switching intervals of the converter. As demonstrated in Fig.3.1, Directly adjusting the energy input to the slowly reacting filter controls the output of the converter. Duty cycle is adjusted to change the energy being input in a feedback configuration, which is basic, uncomplicated, and easy to apply[22]. The converter's dynamic properties are easily predicted and are influenced by mechanism to control duty cycle and the characteristics of filter.

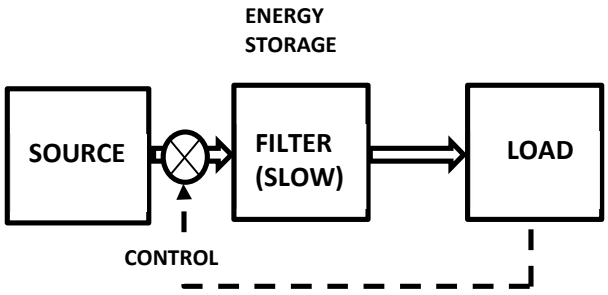

Fig.3. 1 Block Diagram of PWM Converter

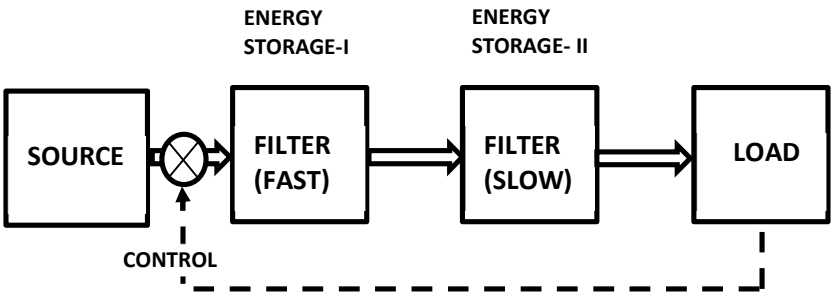

Fig.3. 2 Block Diagram of Resonant Converter

The energy storage elements of resonant converters are slow time constant output filter and a rapid time constant resonant circuit[5], [7], [8], [23]–[25]. As shown in Fig.3.2 resonant tank energy is modulated to regulate output of converter. The resonant tank exchanges massive amounts of pulsating energy with the source and output filter during each half-cycle of converter operation and possess fast dynamics[5], [6], [26]–[28].
Regulation of resonant converters is significantly more difficult than that of PWM counterparts due to the presence of the resonant tank and its fast transient response. The significant current and voltage stresses on components, large power spikes in the resonant tank are few issues needs to be managed by resonant converter control.

Following are the control approaches that have been used on resonant converters [22]:
1) average-current control or analog-signal-to-discrete-time-interval converter (ASDTIC) control
2) frequency control
3) capacitor-voltage control
4) diode-conduction-angle control.

Average current control, frequency control and diode conduction angle control have all been used to control series resonant converters (SRCs), while capacitor voltage control is used to regulate parallel resonant converters (PRCs). Frequency control and optimal trajectory control are mostly used to control LLC resonant converters. Out of many control techniques reported, frequency control is the simpler and easy to implement for LLC converter as the resonant tank impedance can be directly controlled by switching frequency [4], [22]. Also, the relationship between the control signal and frequency shows linear characteristics, which can alleviate the need of complex non-linear controllers.

Soft Starting

Under steady state the converter is operated at the resonant frequency as efficiency of LLC resonant converter is maximum at this frequency. If at the starting, the converter is operated at resonant frequency the resonant tank having minimum impedance act as a short circuit. During this time the converter experiences large inrush current and voltage levels

which if not managed may result into the failure of switches[17], [26]–[29]. To manage such inrush current and high voltage transients at the starting, the converter is operated at 2-3 times the resonant frequency as at higher frequency the resonant tank offers finite impedance. To operate the converter at high frequency, close loop generated gate pulses given to inverter switch during this transient time period is reduced or clipped to prevent the inrush current and voltage level to safely operate the switches in safe operating region. Soft starting can be done by clipping the generated gate pulses into two from the middle.

Load Regulation:

To design the tank parameters, it is necessary to consider the charging load as a passive load. The gain characteristics of LLC resonant converter is shown in the Fig.3.4. At switching frequency greater than resonant frequency, magnetizing inductance get clamped by the output voltage and the circuit behaves as a series resonant tank. With the change in line voltages and/or load condition the output voltage changes. To keep the output voltage fixed at the required level the feedforward control is required to modulate the switching frequency at different line and load conditions[7], [18], [29], [30].

The switching frequency for different load conditions can be precalculated from the Gain plot and thus operating the converter at this precalculated switching frequency at different load condition gives proper load regulation.

Similarly, line regulation can also be controlled with the similar approach of precalculated switching frequency for different line voltages.

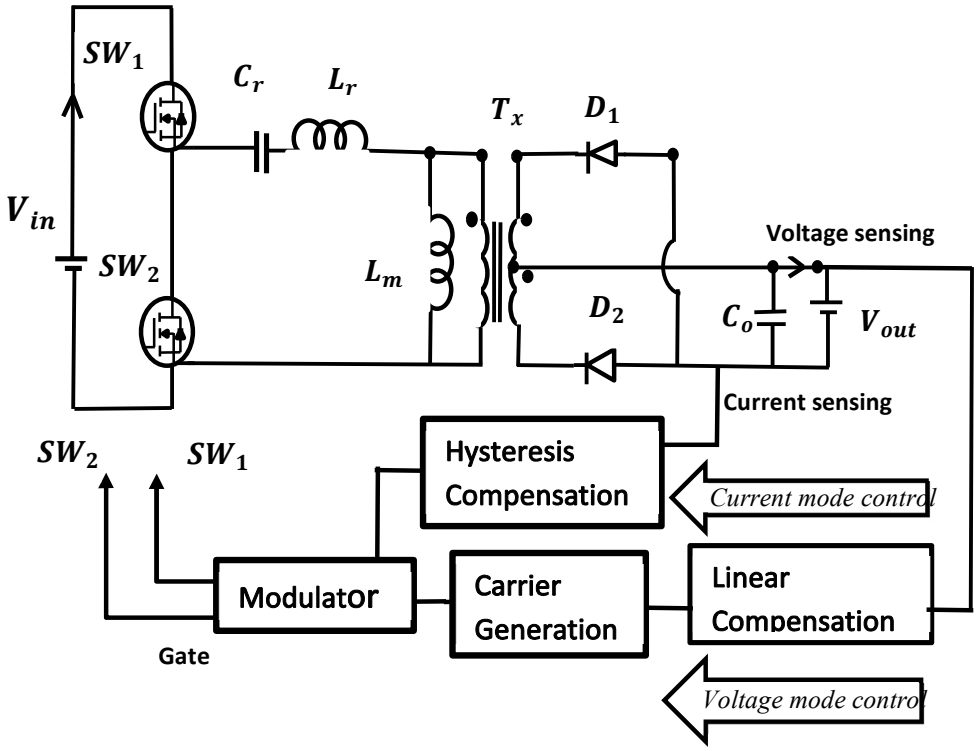

Fig.3. 3 Close loop control of LLC Resonant Converter

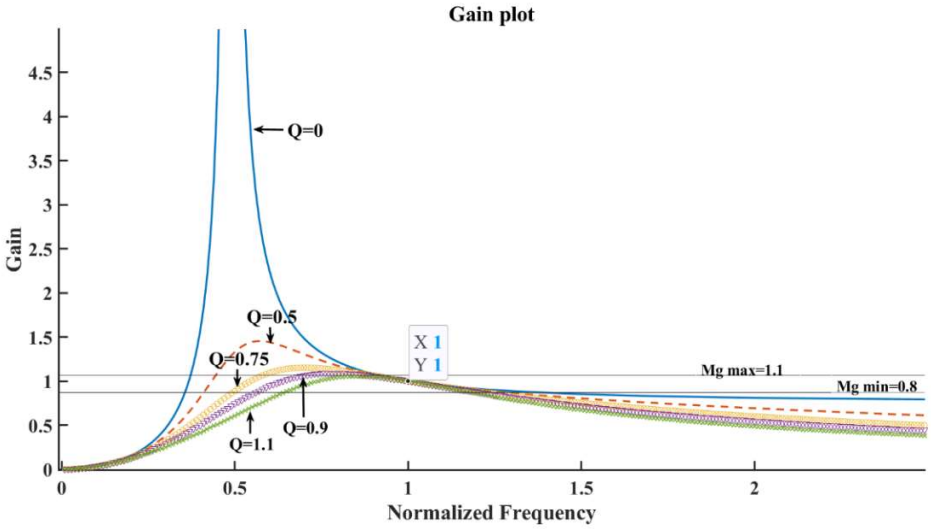

Fig.3. 4 Gain Plot

3.2 Control Algorithm:

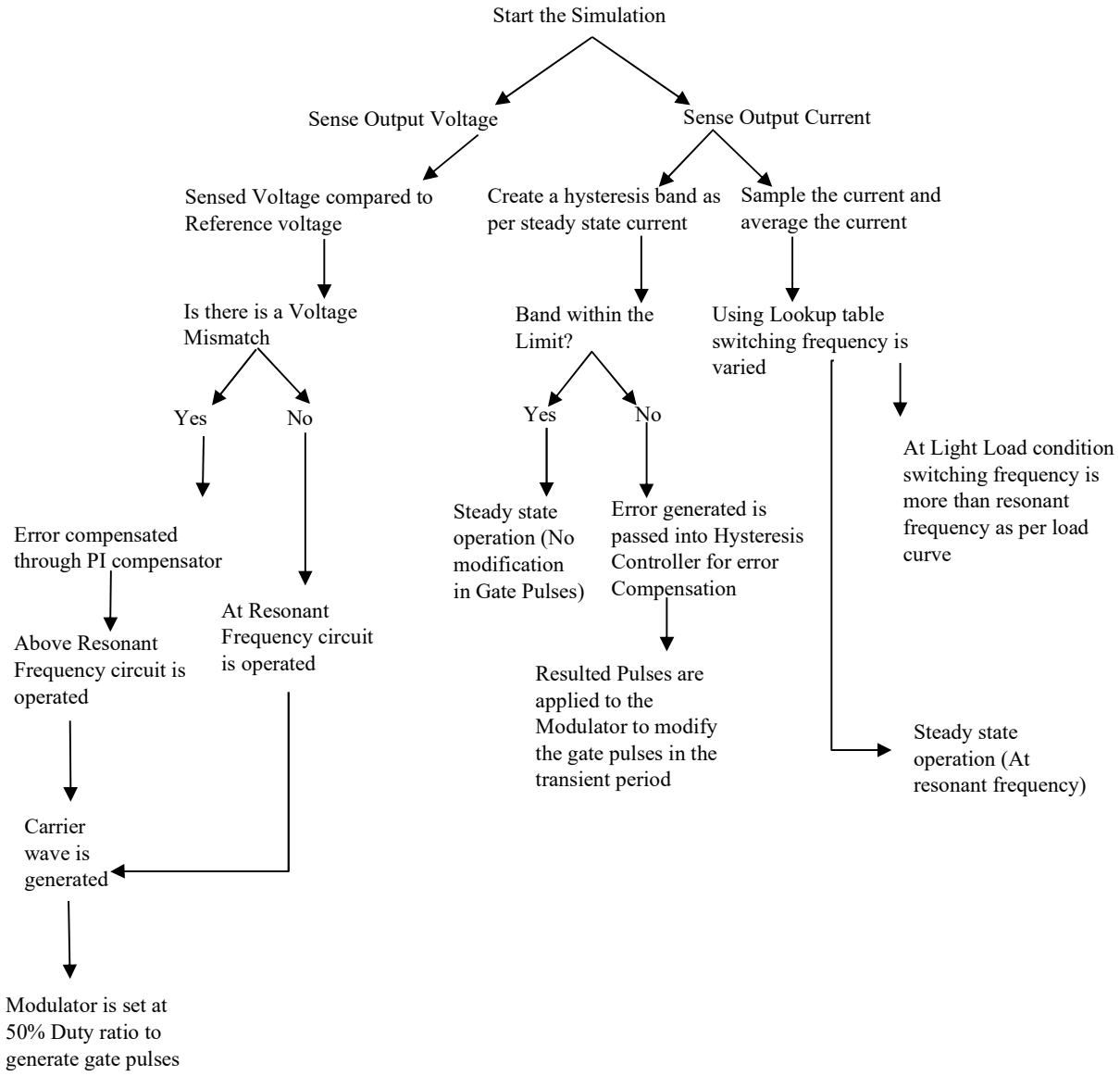

Control Law:

The Proposed topology discusses the On-load start of resonant converter by splitting the converter gating into two and operating at frequency higher than resonant frequency and consequently reducing the switching frequency close to resonant frequency as steady state operation approaches.

Starting the switching frequency at higher value reduces the gate pulse width thus the switches are acting as a filter removing the higher transient present in the current and voltage waveform and safely starting the converter. As steady state operation initiates the switching frequency is reduced to resonant frequency for achieving maximum efficiency. The proposed topology uses Dual control, voltage being regulated through PI compensator and current control being used for determining the switching frequency as per voltage gain curve. Adaptive control is getting achieved as we are able to achieve the switching frequency from the load current and carrier wave is generated at that switching frequency as per different load condition. At high load condition the current is more and so the switching frequency get less than the resonant frequency ($f_{sw} < f_r$). Whereas at light load condition the current is less and so as to maintain the output voltage the switching frequency is more than the resonant frequency ($f_{sw} > f_r$). Load Current is sensed from the output to vary the switching frequency as per the load condition. For this, the load current is averaged and from the look up table corresponding switching frequency is determined in according to the gain curve.

The startup response is one of the important indicators of the controller's capacity to manage big transients, in addition to steady-state performance and the LLC converter's large-signal behavior following disturbances. During startup, the LLC converter's output capacitor behaves like a very heavy load producing an inrush current. Fig.3.3 shows the circuit schematic of an LLC converter, whereas Figure3.4 shows the frequency gain characteristics. Because high switching frequencies diminish the converter's gain, typical starter procedures aim to reduce inrush current by starting the converter at maximum frequency and gradually decreasing it (with a time constant) until the target operating point is reached [6].

3.3 Simulation Results:

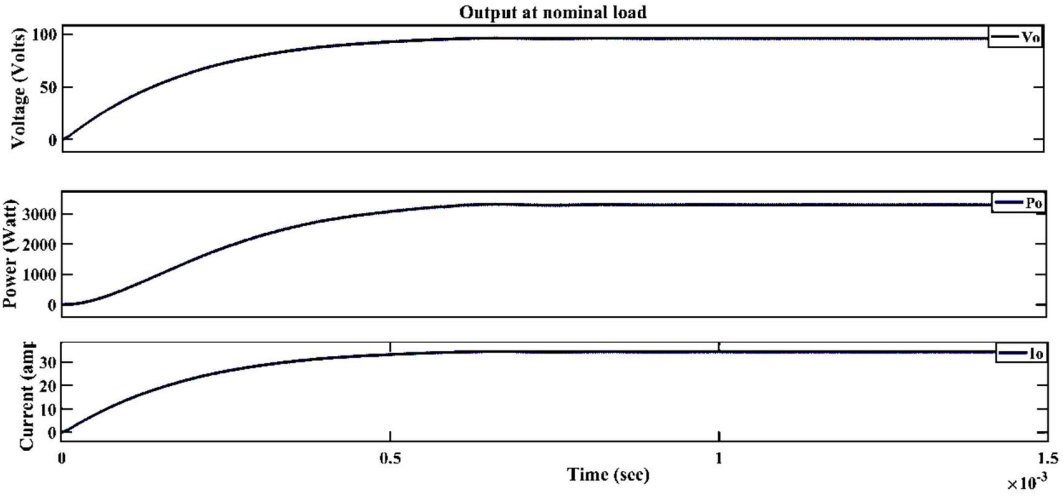

Fig.3. 5 Nominal Load Output

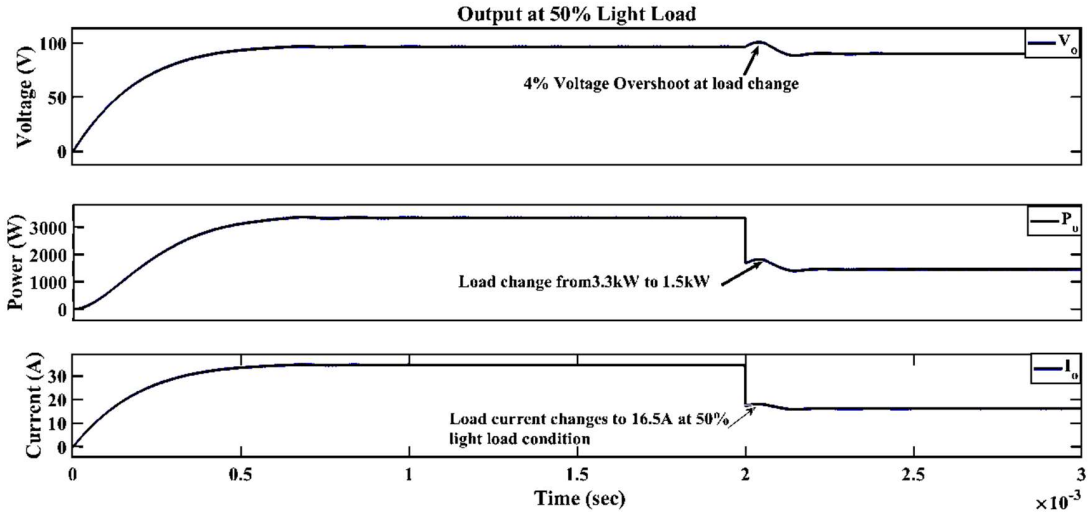

Fig.3. 6 Dynamic Load change from Full load to 50% Light load.

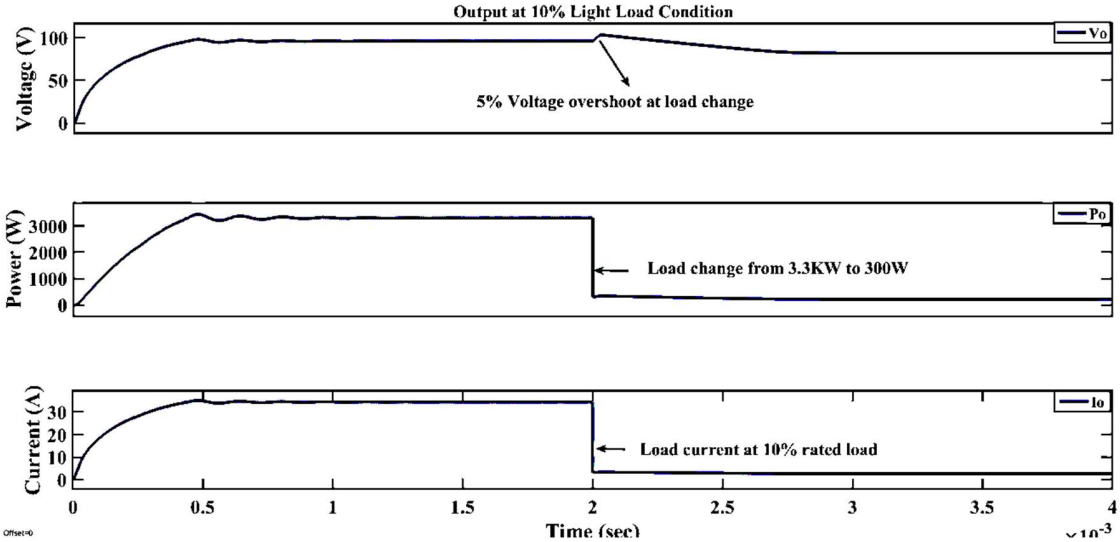

Fig.3. 7 Dynamic Load change from Full load to 10% Light load.

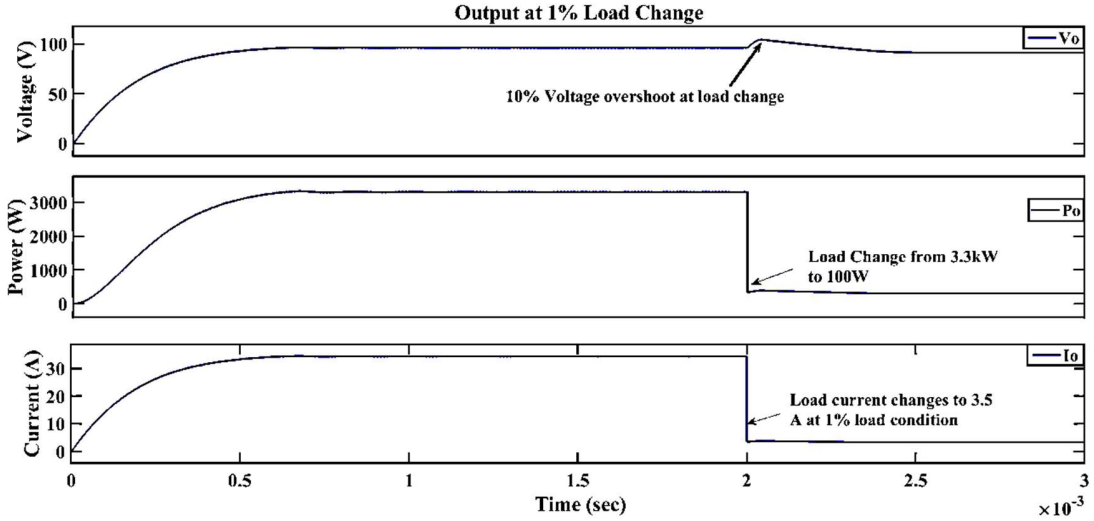

Fig.3. 8 Dynamic Load change from Full load to 1% Light load.

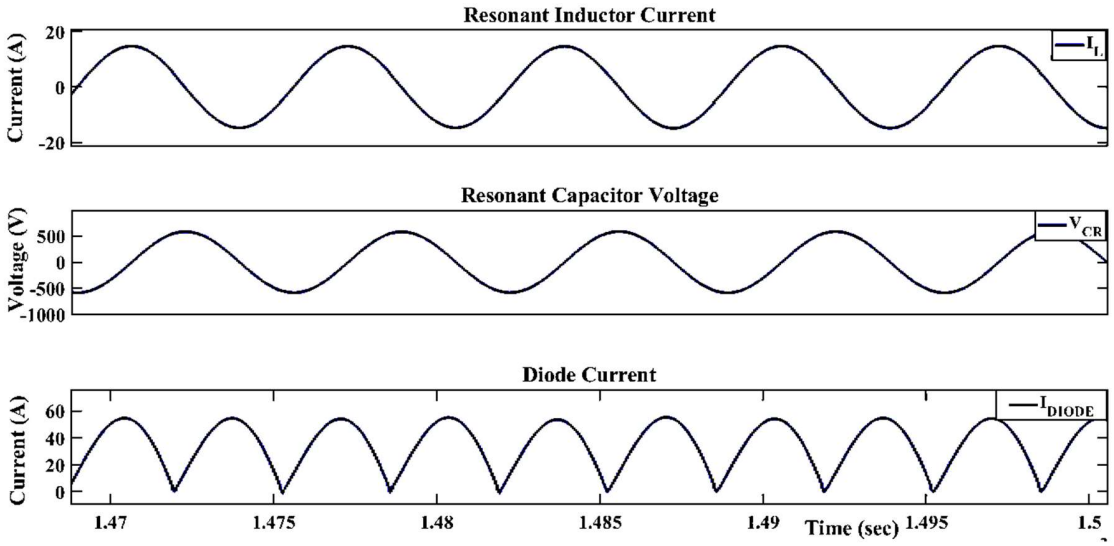

Fig.3. 9 Resonant Tank Parameter Waveform

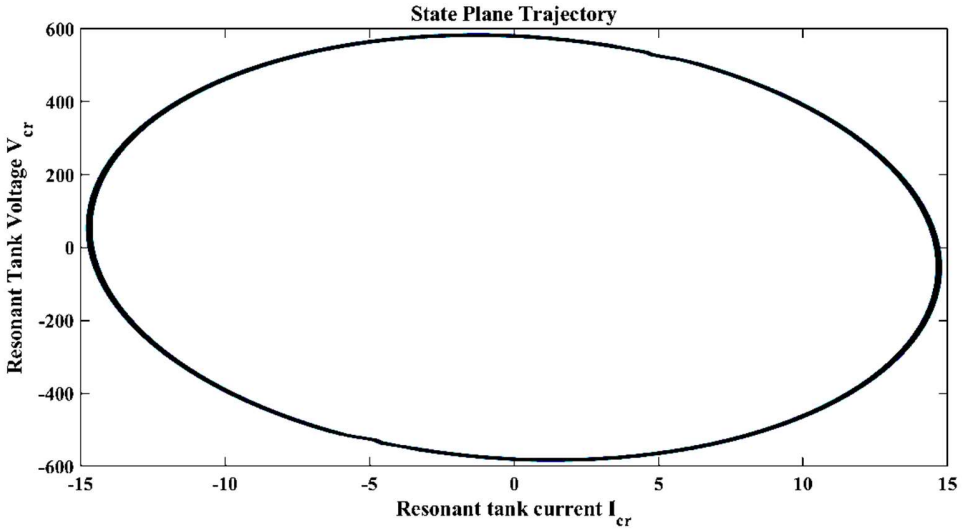

Fig.3. 10 State Plane Trajectory at Nominal Load

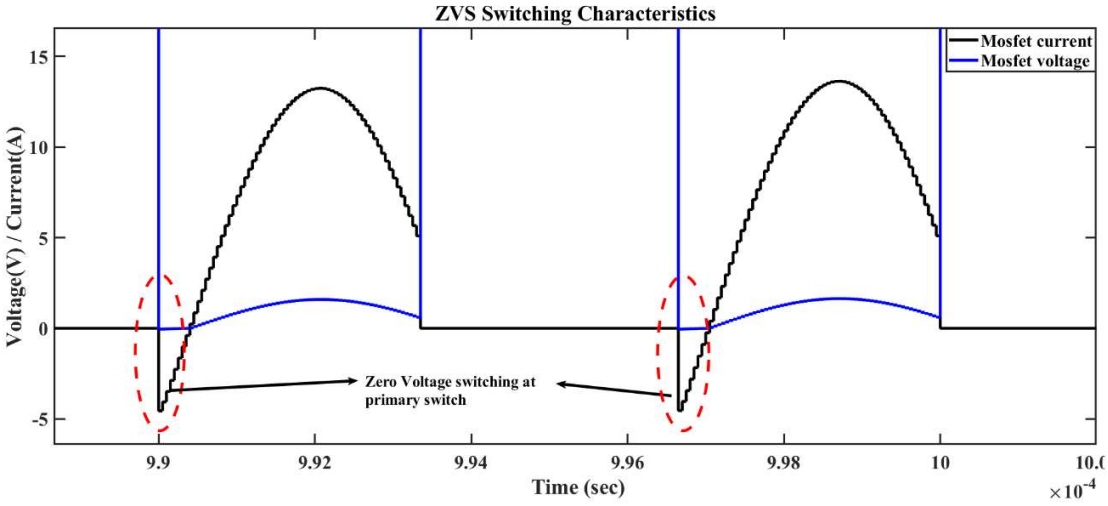

Fig.3. 11 Zero Voltage Switching at primary side MOSFET

CHAPTER 4
CIRCUIT DESIGN AND MAGNETICS DESIGN

4.1. Gain equation:

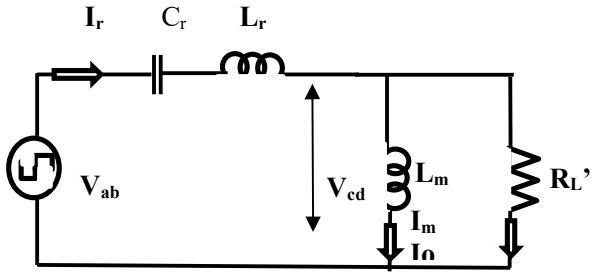

Fig.4. 1 Equivalent Circuit of LLC resonant converter

The input to output voltage gain function is defined as [13],

$$M_g^{dc} = \frac{n * V_{cd}}{V_{ab}/2} \tag{4.1}$$

Based on the Fundamental harmonic approximation (FHA) method, the gain function is approximated by their fundamental voltages,

$$M_{g,1}^{ac} = \frac{V_{cd,1}}{V_{ab,1}} \tag{4.2}$$

FHA-based gain function can be expressed with circuit parameters as,

$$M_g^{dc} = M_{g,1}^{ac} = \left| \frac{(j\omega L_m) /\!/ R_e}{(j\omega L_m) /\!/ R_e + (j\omega L_r) + 1/(j\omega C_r)} \right| \tag{4.3}$$

Equation (4.3) can be expressed in a normalized form; accordingly, the normalized gain function is obtained as:

$$M_g^{dc} = M_{g,1}^{ac}$$
$$= \left| \frac{L_n * {f_n}^2}{[(L_n + 1) * {f_n}^2 - 1] + j({f_n}^2 - 1) * L_n * f_n * Q_e} \right| \quad (4.4)$$

where, f_n is normalized switching frequency: $f_n = \frac{f_{sw}}{f_o} = \frac{2\pi f_{sw}}{2\pi f_o} = \frac{\omega_{sw}}{\omega_o} = \omega_n$, L_n is Normalized inductance ratio: $L_n = \frac{L_m}{L_r}$ and Q_e is the quality factor of the series resonant tank: $Q_e = \frac{\sqrt{L_r/C_r}}{R_e}$.

Static Gain without load

The processing power is zero when the converter is not in use. The parametrized load current is zero in this scenario. As a result, static gain, defined as

$$M = \frac{({f_n}^2)}{{f_n}^2(L_n + 1) - L_n} \quad (4.5)$$

It is established that when $f_n > 1$, static gain is less than one and static gain is bigger than one, and when $f_n < 1$.

The converter will even function without a load and its voltage can be regulated by the switching frequency.

Static gain as function of load resistance

The expression

$$M = \frac{\sqrt{{f_n}^4 - \left[\pi^2/8\,[f_n^2 - 1]\bar{I}_o'\right]^2}}{{f_n}^2(L_n + 1) - L_n} \quad (4.6)$$

The expression shows static gain as a function of a parametrized value of average load current reflected to the transformer's primary side.

4.2 Parameter Design:

Transformer's turns ratio:

$$n = M_g * \frac{V_{in}}{V_{out}} = \frac{V_{in}}{V_{out}}\Big|_{M_g=1} = 4.17 \approx 4 \tag{4.7}$$

Minimum Gain (M_{gmin}):

$$M_{gmin} = n * \frac{(V_{o\_min} + V_F)}{V_{in\_max}} = 4 * \frac{(96 * (1 - 5\%) + 0.7)}{415} = 0.885 \tag{4.8}$$

where, V_F is forward voltage drop across switch

Maximum Gain (M_{gmax}):

$$M_{gmax} = n * \frac{(V_{o\_max} + V_F)}{V_{in\_min}} = 4 * \frac{(96 * (1 + 5\%) + 0.7)}{380} = 1.08 \tag{4.9}$$

The values of the Quality factor and inductance ratio are selected such that the resulting gain curve plot drawn should cut the maximum gain value and minimum gain value designed for frequency range above the resonant frequency for ensuring ZVS operation. The gain plot is presented in Fig. 2. Accordingly Quality factor, $Q_e = 1.1$; Inductance ratio, $L_n = 3.2$; equivalent resistance, $R_e = \frac{8*n^2}{\pi^2} * \frac{V_o}{I_o} = 36.22\Omega$ and at 110% Loading $R_e = 32.92\Omega$; the chosen resonant frequency $f_r = 150$kHz; Hence the resonant capacitor $C_r = \frac{1}{2\pi*Q_e*f_r*R_e} = 26.6$ nF ; resonant inductor $L_r = \frac{1}{(2\pi*f_r)^2*C_r} = 42.3$ µH ; and magnetizing inductor $L_m = L_n * L_r = 135.36\mu$H.

The switch is selected as per the feasible dead time which is given by:

$$t_d \geq 16 * C_{eq} * f_{sw} * L_m \geq 104\text{nsec} \tag{4.10}$$

Minimum Frequency:

$$f_{smin} = M_{gmin} \times f_r = 0.885 \times 150\ kHz = 132\text{kHz} \tag{4.11}$$

Maximum Frequency:

$$f_{smax} = M_{gmax} \times f_r = 1.08 \times 150\,kHz = 162\text{kHz} \quad (4.12)$$

Primary side load current (I_{oe}):

$$I_{oe} = \frac{\pi}{2\sqrt{2}} \times \frac{1}{n} \times I_o = 9.54\text{ A} \quad (4.13)$$

Secondary side load current (I_{oe_s}):

$$I_{oe\_s} = I_{oe} \times n = 38\text{ A} \quad (4.14)$$

Primary side magnetizing current (I_m):

$$I_m = 0.9 \times \frac{nV_o}{\omega L_m} = 2.72\text{ A} \quad (4.15)$$

Resonant Tank Current (I_r):

$$I_r = \sqrt{I_{oe}^2 + I_m^2} = \sqrt{9.54^2 + 2.72^2} = 9.9\text{ A} \quad (4.16)$$

Table 4. 1 Designed LLC Resonant Converter Parameters

Parameter	Designator	Value
Transformer Turns Ratio	n	4
Minimum Gain	M_{gmin}	0.885
Maximum Gain	M_{gmax}	1.05
Quality factor	Q_e	1.1
Inductance ratio	L_n	3.2
Equivalent resistance	R_e	36.22Ω
Resonant capacitor	C_r	26.6 nF
Resonant Inductor	L_r	42.3µH
Magnetizing Inductor	L_m	135.36µH
Dead time	t_d	104nsec
Minimum Frequency	f_{smin}	132kHz
Maximum Frequency	f_{smax}	164kHz
Primary side load current	I_{oe}	9.54 A
Secondary side load current	I_{oe_s}	38 A
Primary side magnetizing current	I_m	2.72 A
Resonant Tank Current	I_r	9.9 A

For the designed tank parameters, the switching frequency is kept greater than resonant frequency, thus magnetizing inductance gets clamped by the output voltage for heavy load conditions and the circuit behaves as a series resonant tank and aids ZVS. Thus, with the change in line voltages and/or load condition the output voltage changes. To keep the output voltage fixed at the required level the feedforward control becomes requisite to modulate the switching frequency at different line and load conditions. The switching frequency for different load conditions can be precalculated from the gain plot and thus operation of the converter at this precalculated switching frequency is stored in a 2-D array for lending support to closed loop control without losing time for calculations at different load condition offer proper load regulation. Similarly, line regulation can also be controlled by precalculated switching frequency for different line voltages acquiring input from 2-D array and closed loop proposed control.

4.3 Magnetics design:

The conversion process in power electronics demands the use of transformers and components, which are frequently the heaviest and bulkiest components in the conversion circuit. They also have a significant impact on the overall performance and efficiency of the system. As a result, the weight, efficiency, and cost of the overall system are all affected by the design of such transformers. Because of the complexities and influence of various of parameters, rational compromises are necessary to meet design optimization[31].

The primary purpose of increasing the switching frequency is to reduce the size of the passive components. The transformer in a standard LLC converter can take up almost half of the converter's footprint. As a result, reducing the transformer size increases the converter power density significantly. To reduce winding and switching losses, modern industrial solutions use relatively low frequency designs in the region of ~200 kHz. Litz wire windings are preferable for this range of frequency. Low-frequency designs can achieve high efficiency, but they are bulky and labor-intensive to manufacture. With the Wide Band Gap devices such as SiC and GaN, it was feasible to increase switching frequency without sacrificing switching loss. By increasing the switching frequency to the order of MHz, the transformer size will reduce substantially [32].

TRANSFORMER DESIGN USING A_p approach:

The user is most concerned with the output power, P_o. The apparent power, P_t, which is related to the transformer's shape, is more important to the transformer designer. Assume that the core of an isolation transformer contains only two windings in the window region, a primary and a secondary, for the purpose of simplicity. Assume that the window area (W_a), is divided proportionally to the windings' power-handling capability, with equal current density. The load's primary winding handles, P_t, and secondary winding handles, P_o.

By definition:

Apparent Power (P_t):

$$P_t = P_{in} + P_o \tag{4.17}$$

$$P_{in} = \frac{P_o}{\eta} \tag{4.18}$$

where, η is the efficiency of the converter

Primary turns can be expressed using faraday's law:

$$N_p = \frac{V_p(10^4)}{A_c B_{ac} f K_f} \tag{4.19}$$

Winding area of transformer is fully utilized when:

$$K_u W_a = N_p A_{wp} + N_s A_{ws} \tag{4.20}$$

By definition, the wire area is:

$$A_w = \frac{I}{J} \tag{4.21}$$

Rearranging the equation shows:

$$K_u W_a = N_p \frac{I_p}{J} + N_s \frac{I_s}{J} \tag{4.22}$$

Substitute the faraday law:

$$K_u W_a = \frac{V_p(10^4)}{A_c B_{ac} f K_f}\left(\frac{I_p}{J}\right) + \frac{V_s(10^4)}{A_c B_{ac} f K_f}\left(\frac{I_s}{J}\right) \tag{4.23}$$

Rearranging

$$A_c W_a = \frac{(V_p I_p + V_s I_s)(10^4)}{B_{ac} f K_f K_u J} \tag{4.24}$$

By definition,

$$P_{in} = V_p I_p \tag{4.25}$$

$$P_o = V_s I_s \tag{4.26}$$

$$P_t = V_p I_p + V_s I_s \tag{4.27}$$

$$A_c W_a = \frac{(P_t)(10^4)}{B_{ac} f K_f K_u J} \tag{4.28}$$

$$A_p = A_c W_a \tag{4.29}$$

$$A_p = \frac{(P_t)(10^4)}{B_{ac} f K_f K_u J} \tag{4.30}$$

Limitations with High Frequency Converters [32]:

The core and winding losses make up the magnetic loss.

The core loss and size can be reduced by raising the frequency, but the ac winding loss increases. Low voltage high current applications, such as those used in telecommunications and server applications, have extremely high output currents (ranging from 70 A to more than 100 A), causing problems for the LLC circuit.

1) Under high current, SR devices become thermally stretched, necessitating the employment of parallel devices. The parasitic inductances in the parallel connections generate current sharing concerns amongst parallel devices, so paralleling devices at high frequencies is challenging.

2) The secondary winding is put under a lot of strain when there's a high frequency and high current. To cut down on conduction loss, parallel winding turns are also essential. This technique, however, necessitates a large number of layers on the PCB, which is prohibitively expensive.

3) The termination point between parallel transformer windings and SR devices passes a large amount of current at a high frequency. The termination connection's lack of interleaving and high leakage inductance raises ac resistance, resulting in a large termination loss.

4) On the transformer winding, a high switching frequency results in a high dV/dt rate. The interwinding capacitance allows more common mode (CM) current to flow from the primary to the secondary side. It's also difficult to control EMI in high-frequency devices.

To handle such high current at high frequency, foil winding is most prominent solution

Using Core Geometry Approach:

Table 4. 2 Transformer Design Parameter

Parameter	**Designation**	**Value**
Input Voltage	V_{in}	380 V
Output Voltage	V_o	96 V
Frequency	f	150 kHz
Efficiency	$\boldsymbol{\eta}$	98%
Regulation	α	0.5
Diode voltage drop	V_d	1 V
Flux density	B_{ac}	0.05 Tesla
Window Utilization Factor	K_u	0.6
Core Material		Ferrite

Transformer Output Power P_o,

$$P_o = I_o \times (V_o + V_d) = 34.375 \times (96 + 1) = 3334.375\ W \tag{4.31}$$

Total secondary apparent power P_{ts},

$$P_{ts} = P_o \times U = 3334.375 \times \sqrt{2} = 4701.5W \tag{4.32}$$

Transformer Input Power P_i,

$$P_i = \frac{P_o}{\eta} = \frac{3334.375}{0.98} = 3402W \tag{4.33}$$

Total primary apparent power P_{tp},

$$P_{tp} = P_i \times U = 3402 \times \sqrt{2} = 4811W \tag{4.34}$$

Total apparent power P_t,

$$P_t = P_{tp} + P_{ts} = 9512.5W \tag{4.35}$$

Electrical Condition K_e,

$$K_e = 0.145 \times K_f^2 \times B_{ac}^2 \times f^2 \times (10^{-4}) = 0.145 \times 4^2 \times 0.05^2 \times 150000^2 \times (10^{-4}) = 13050 \tag{4.36}$$

Core Geometry K_g,

$$K_g = \frac{P_t}{2 \times K_e \times \alpha} = 0.594 \tag{4.37}$$

Selected Core comparable to core geometry:

Table 4. 3 Selected Core and its parameters

Parameter	Designation	Value
Selected core	TDK	ETD44
Effective cross section of the core	A_c	2.11 cm^2
Area product	A_p	3.434 cm^4
Core geometry coefficient	k_g	0.5937 cm^5
Window area	W_a	3.434 cm^2
Mean length turn	MLT	10.3 cm

CHAPTER 5

TRANSIENT HANDLING IN LLC RESONANT CONVERTER

5.1 INRODUCTION

Resonant converter faces large transient during dynamic load change due to fast dynamic response of the resonant tank, non-linearity linked with rectifier and non-linearity linked with Variable control oscillator (VCO). Beside this, at staring the converter witness a large inrush current and voltage stresses on primary switches which may lead to permanent damage to the switches [2], [6,7], [17], [30], [33], [34]. Optimal trajectory control is presented in the literature to demonstrate effective operation, but due to involvement of complex mathematical expressions, duly aided by multiple sensors become tedious to implement on fixed point microcontrollers [5,13]. Average geometric control is discussed in literature [6,7] which is based on average large signal model to predict large signal behavior and consequently controls the transients with large computations. The proposed scheme focuses on simplifying the control scheme for implementation on inexpensive fixed-point microcontroller by avoiding the complex mathematical expressions and geometric modeling-based algorithm by using preventive measures to mitigate the inrush current during transients. The transient conditions are handled.

The proposed scheme focuses on simplifying the control scheme for implementation on inexpensive fixed-point microcontroller by avoiding the complex mathematical expressions and geometric modeling-based algorithm by using preventive measures to mitigate the inrush current during transients. The transient conditions are handled through new method by splitting the gate pulses into two halves the propose scheme, thus operating the converter at switching frequency twice the resonant frequency along with variable pulse width, utilizing the increased impedance due to double frequency to limit current and pulse width modulation for voltage magnitude control. Variable Frequency control of the LLC converter is exercised through 2-D look up table along with simple PI controller to customize the operation amidst load perturbation.

5.2 Pulse Splitting Cum Width Control:

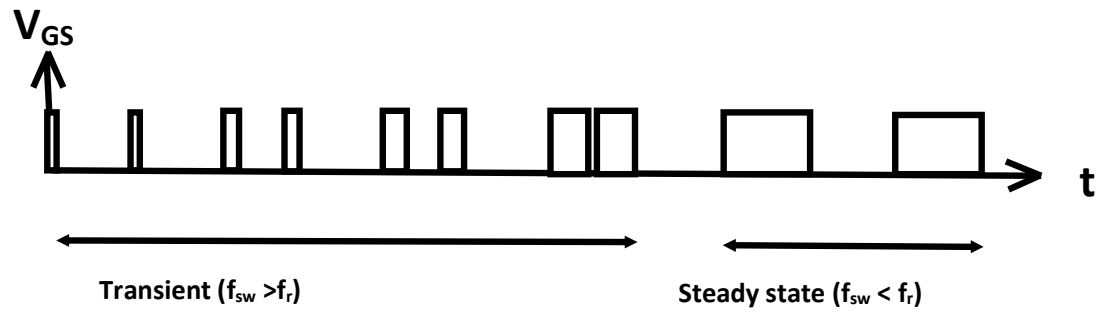

Fig.5. 1 Proposed Gate Pulses

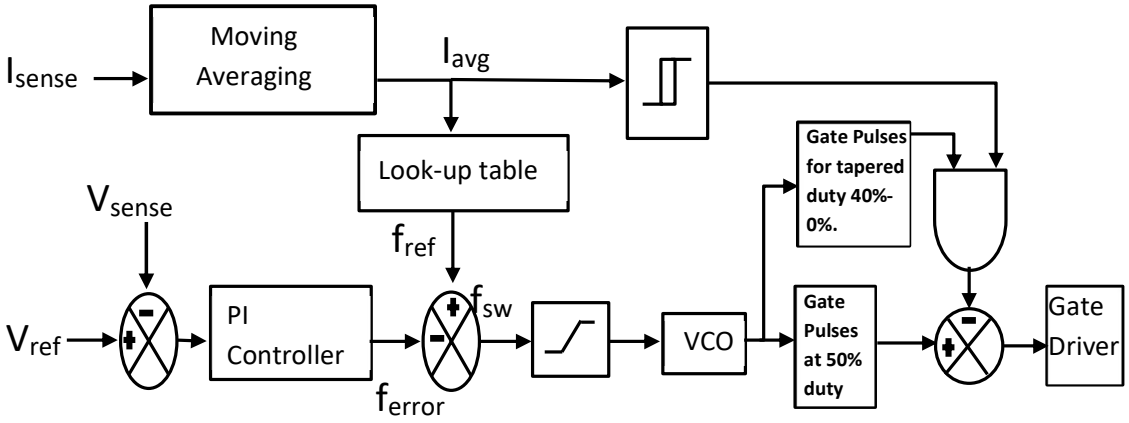

Fig.5. 2 Block Diagram of control scheme incorporating proposed transient handling control

Control Scheme:

The proposed controller employs closed loop frequency control since the relationship between frequency and control signal is linear, thereby giving liberty to use linear PI controller effectively, and avoiding complexity implemented on costly DSP controllers. The block diagram depicting the control logic is as shown in the Fig.4. The steady state control is implemented as voltage controlled derived frequency control realized through the PI controller. ferror computed by PI controller in addition to feedforward switching frequency ffeedforward component derived from the 2-D look up table holding the data of switching frequency corresponding to different load current values and different input voltage loading forms the reference frequency value designated for resonant tank excitation. Feedforward control offer faster dynamics of the converter. Finally using the VCO, the gate pulses are generated at near 50% duty ratio including the dead time value requisite for discharge from output capacitance of the switch provoking the antiparallel diode to invoke ZVS of primary side switches. Under steady state, the converter is operated at the resonant frequency as efficiency of the LLC resonant converter is maximum at this frequency. During transients, if converter is continued to operate near resonant frequency it is bound to experience large inrush current and unwanted voltage levels in the resonant tank which if not managed may result into the failure of switches. To manage such situation, the reported literature suggests the converter is operated at 2- 3 times the resonant frequency, thereby bringing in substantial impedance to the resonant tank. To operate the converter at such high frequency, gate pulses are generated under closed loop control, thus during transient period only reduced or clipped level of inrush currents are allowed in the resonant tank. The proposed control during transient conditions is invoked by chopping the generated gate pulses into two from the middle as shown in the Fig. 5. The transient state control is made to work in current control by averaging the sensed current and its level monitored thereof. Any transient condition at near resonant frequency raises the current level which is readily detected, and the same is differentiated from steady state condition. The VCO, which earlier was entrusted to generate 50% duty at particular frequency now generates a tapering duty output also starting from near 40% to 0%. Such

tapered duty were ANDed and subtracted from 50% duty waveform producing the splitting of pulses at double frequency as shown in the Fig. 5. Such pulse width modulated double frequency pulse not only act on limiting the inrush current through increased resonant tank impedance, but also control the voltage due to modulated pulses.

The LLC converter's large signal behavior may be shown to be linear at the resonant frequency, as shown in part in Fig. 1. (b). The LLC converter's normalized voltage gain is 1 for all loading conditions except no load, as seen in this diagram. At the resonant frequency, the LLC converter has two working modes, as shown in Fig. 1 (c) and (d) (d). The resonant frequency can be calculated using the formula below: The large-signal behavior of the LLC converter is linear on average when it works at the resonant frequency. The LLC converter's large-signal dynamic behavior can be investigated after applying a step input voltage with no load.

$$f_r = \frac{1}{2\pi\sqrt{L_r C_r}}$$

$$t_k = \pi\sqrt{L_r C_r}$$

Performance Evaluation:

During on-load start of high-power converter system, the issue of handling inrush current dominates. The proposed control logic is validated through MATLAB simulation results for transient conditions. The Converter is shown supplying the load of 3.3kW at 96V from 380V DC Bus. The parameters of resonant tank circuit are Lr=42.3µH, Lm=136µH and Cr=26.6n which is operating closely above the resonant frequency of 150kHz. Two types of transient responses are investigated in our study; the starting response where the magnetic circuit is routed along with sudden loading of source, transition from no load to full load and full load to no load. Fig.5.3 depicts converter tank response waveform while looping the operation of tank circuit at around resonant frequency. It may be observed that transient peak voltage may go up to 3KV, and the peak current may mount up to 75A, while diode current may witness two peak curves of 300A. Usually frequency is changed from 2-3 times the resonant frequency and a complex tracking control is employed to bring

the frequency back near resonant frequency to limit the inrush current by increasing impedance. The starting transient response of LLC resonant converter using the proposed control logic is as shown in the Fig. 5.4 It may be observed that by splitting the pulses eventually frequency goes double, besides reduction in pulse width. It is clear from the Fig. 5.4 that inrush current is very well contained below 50A and voltage across output rises to its steady state without any ripple. As proposed in the control logic it can be observed in the Fig. 5.4 at no load start of LLC resonant converter, the gate pulse Vgs is split into two half indicating operation at the twice the resonant frequency with limiting the inrush tank current with fast transient settling time, ts=400µsec and rise time of tr=350 µsec. Similarly transient current limitation is depicted in Fig. 5.5 where load transition of LLC resonant converter is made from no load to full load using proposed control logic. It may be observed that the control logic enables the transient's settlement in 1ms and keeping the peak current well within 20A. While observing similar response shown in Fig.5.6, where load transition is made from full load to no load and its transient settling in time, ts=50 µsec. For depiction of the outlined control the state plane trajectory is shown in Fig. 5.7 with decreasing radii depicting decrease in transient energy, while settling down to normal operating conditions.

5.3 SIMULATION RESULTS:

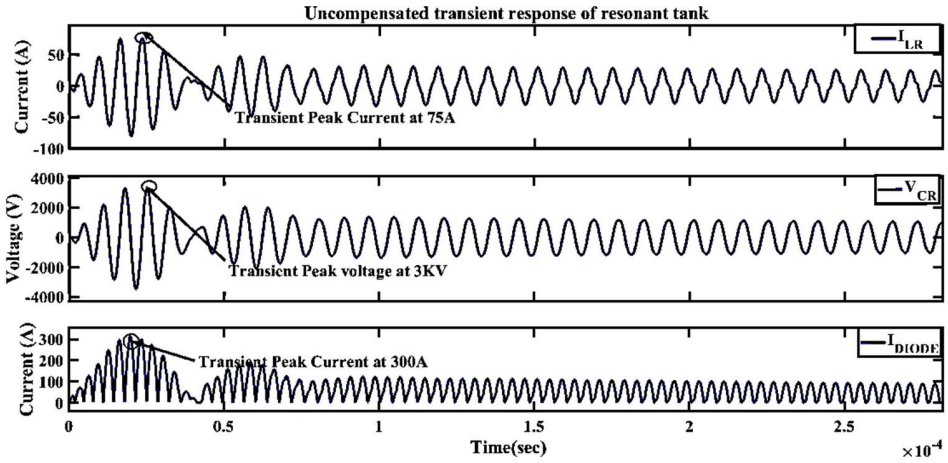

Fig.5. 3 Converter Tank response waveform without proposed controller

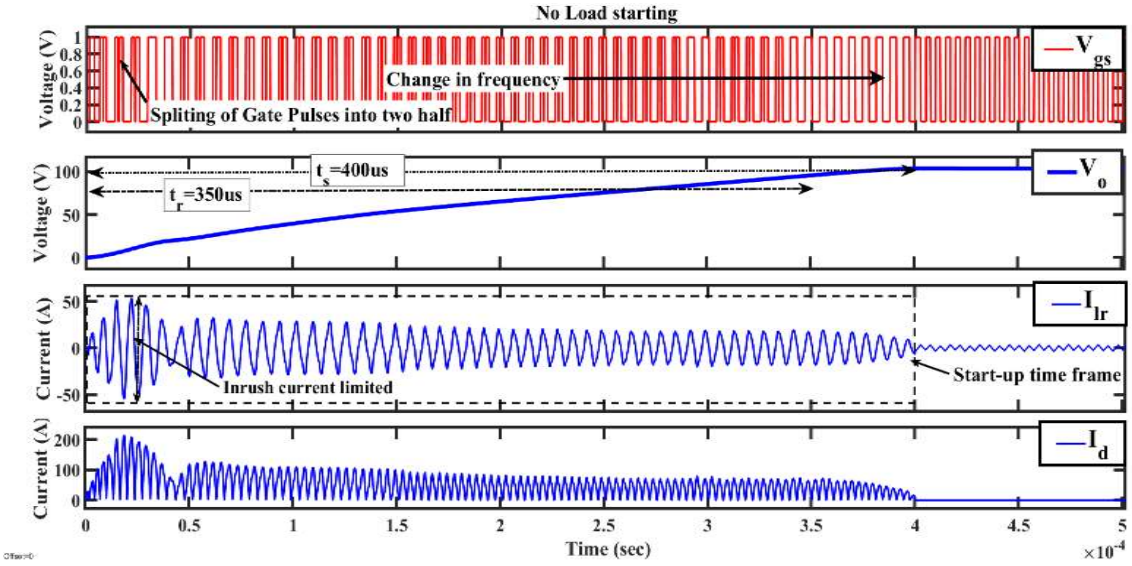

Fig.5. 4 The transient response of LLC resonant converter under the proposed control logic at No load start-up

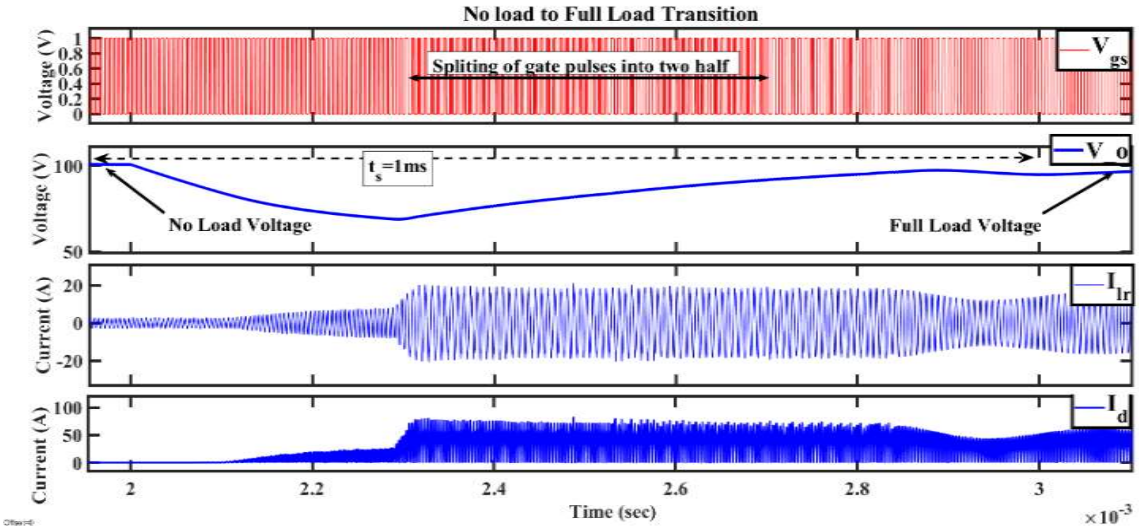

Fig.5. 5 The transient response of LLC resonant converter under the proposed control logic at full load to no load transition

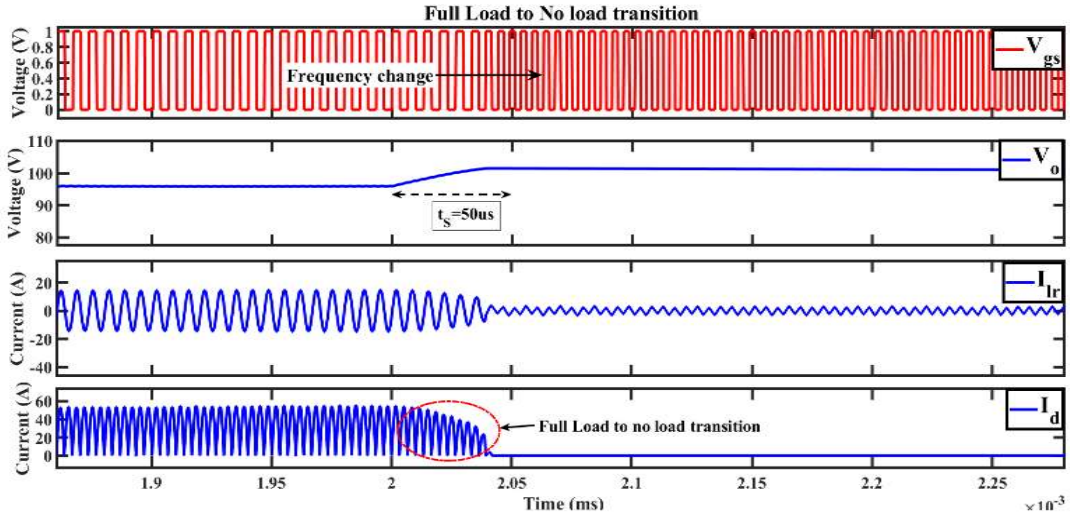

Fig.5. 6 The transient response of LLC resonant converter under the proposed control logic under no load to full load transition

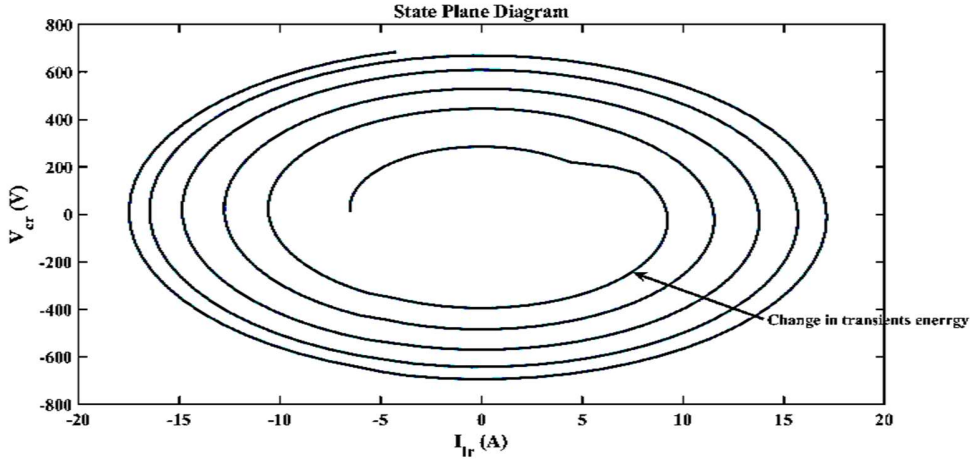

Fig.5. 7 State Plane Trajectory during inrush current control

5.4 Chapter Summary:

A new pulse splitting control technique with hybrid control for handling transients in a LLC resonant converter has been investigated. The observed performance of the pulse splitting cum PWM has demonstrated the seamless handling of transients even at full load conditions. The demonstrated results conform the containment of inrush current to the tank circuit within limits without exercising complex control and costly dsp controllers for its implementation. A simulation study has been conducted and has validated the effectiveness of the proposed scheme. It has also been observed that the proposed scheme has a fast response to load perturbations and starting transients and is able to restrict the flow of unwarranted current in the tank circuit by swiftly splitting the pulses and controlling the width of the pulses for the safety of the switches. During steady state operation, the switching frequency smoothly transacts near resonant frequency for achieving maximum efficiency. Simulation results of 3.3KW LLC resonant converter validates the theoretical analysis. The scheme has the advantage of flexibility of increasing the impedance of the tank circuit together with control of pulse (a) (b) (c) (d) Fig. 7 Transient response of LLC resonant converter under the proposed control logic: (a) at No load start-up; (b) full load to no load transition; (c) no load to full load transition; and (d) State Plane Trajectory width to handle the transient power. The scheme in general may be applicable to other topologies of resonant converters.

CHAPTER-6
DUAL INPUT DOUBLE TANK LLC CONVERTER

6.1 Overview

The World is witnessing a paradigm shift towards eV/HeV/PHeV from fossil/fuel-based engines. The range anxiety is the biggest deterrent for their greater adoption[23], [24]. Since the quantum of high energy density batteries is limited by total volume/weight of the eV, bottleneck gets zeroed down to omnipresent charging stations and their fast-charging capabilities[34]–[36]. In developing countries like India where power infrastructure is not uniform throughout the country. The need for off grid EV chargers is essential for wider acceptance of EV/HEV's. Off grid PV fed EV chargers could be a possible solution to range anxiety for EV's in remote areas and rural areas**,** it could offer resilience against grid outages and could be used to deliver power during emergency response and natural disaster/ calamity.

Even, Big Solar farm could be installed for providing fast-charging solution.

Over the years LLC Converter have been seen as industry standard for its usage in fast charging stations due to high efficiency, high power density, wide load and line regulations and rugged operation exhibited by resonant circuits [1,4,6,7,8]. Control of LLC resonant converter however exhibits a challenge owing to quick resonant tank response and non-linearity of output rectifier. Optimal trajectory curve is presented in the literature, but the same is difficult to implement due to complex mathematical equations, duly aided by multiple sensors [5,13]. Load feedback linearization [12] also shares similar difficulties in implementation, putting technology adoption a bit difficult and costly, leaving charging station behind in jeopardy. Variable frequency control is most commonly adopted control technique in LLC resonant converter.

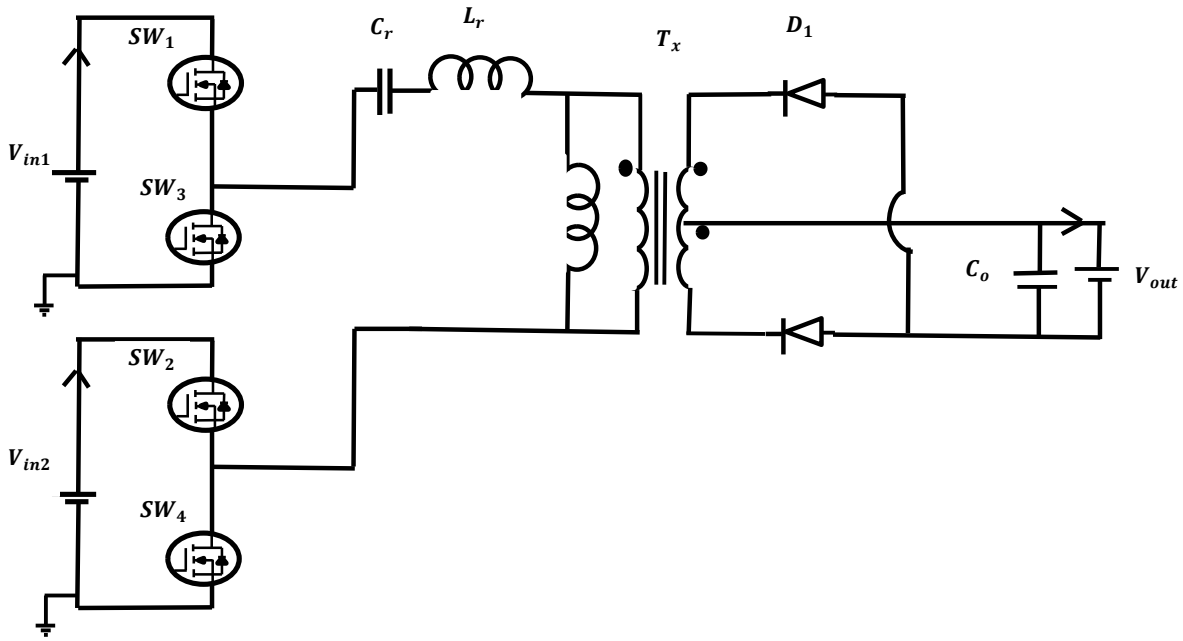

Fig.6. 1 Novel Dual Input common tank resonant converter

6.2 Circuit Analysis

Fig.6.1 exhibits schematic of the proposed PV fed dual input resonant charger, which utilizes single resonant LLC tank to channelize energy in resonant mode, a mid-point tapped rectifier and output filter. This topology has two operating modes, during first mode switch SW_1 and SW_3 are conducting whereas switch SW_2 and SW_4 are switched off and during second mode switch SW_3 and SW_4 are conducting whereas SW_1 and SW_3 are switched off. Each pair of primary side (SW_1, SW_3 and SW_2, SW_4) switch operates at a duty of 50% for each half cycle of the converter's operation. Since direction of current in each half cycle reverses through magnetizing inductor, the topology essentially is operating in the differential mode. The differential mode current in the magnetizing inductor essentially reduces the radiated emissions in high power multilevel circuitry and in digital control circuitry. Primary side switches are switching at zero voltage condition throughout the converter operation as shown in the Fig.6.2 and secondary side diodes are switched at zero current condition throughout the converter operation as shown in the Fig.6.3.

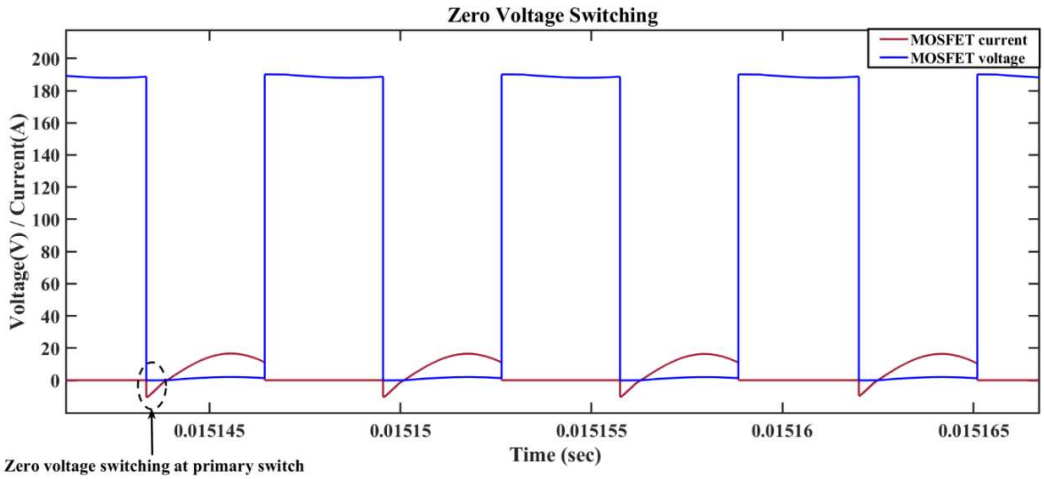

Fig.6. 2 Primary side MOSFET switching at zero voltage

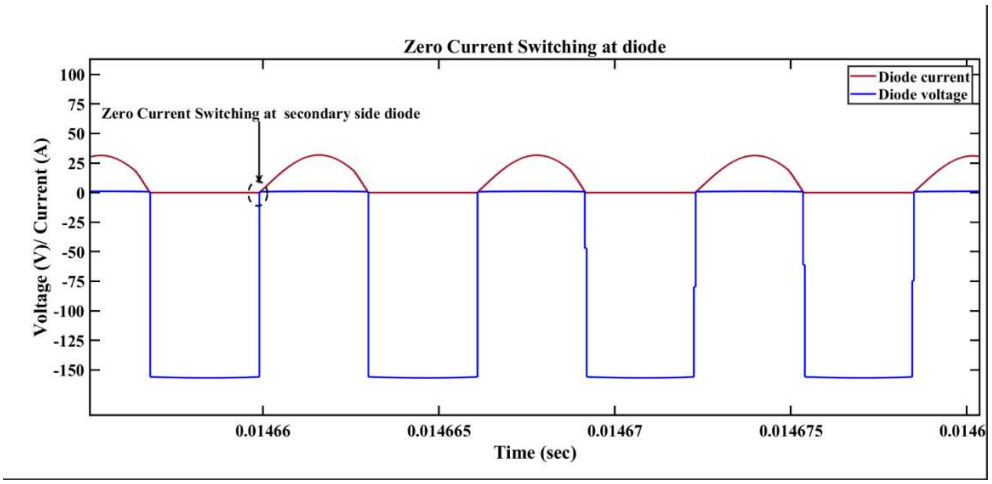

Fig.6. 3 Secondary side Diode switching at zero current

The voltage stress across the primary switch is not more than the input voltage range since each source delivers 50% load. Similarly, the voltage stress across the secondary side diode is twice the output voltage because of the center taped configuration at the output. The source input current waveform is shown in the Fig.6.4. The converter is operating in the constant current control mode with variable frequency control. Differential mode current flowing through magnetization leg further aids in the fast control using simple PI controller as shown in the Fig.6.5.

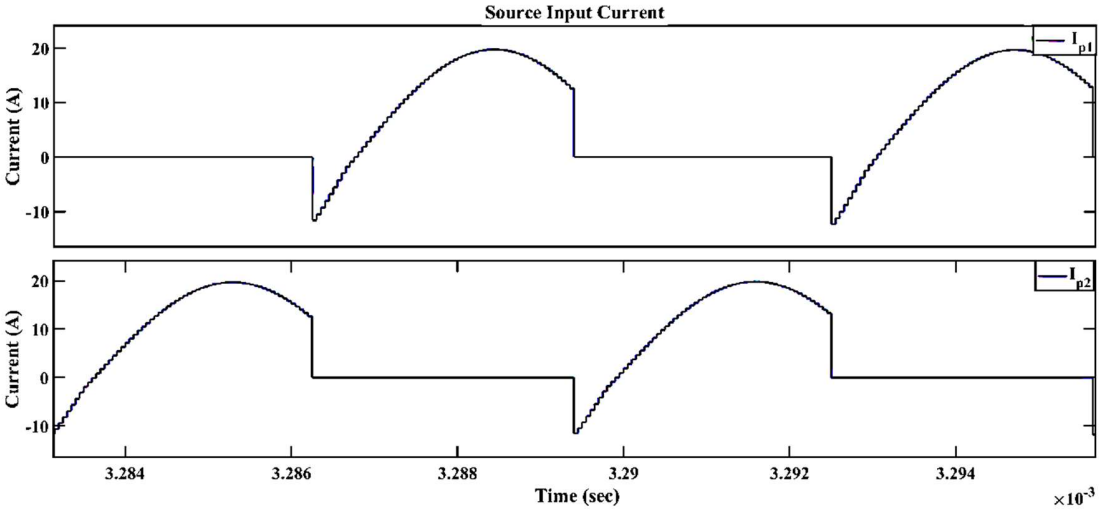

Fig.6. 4 Input Source current waveform

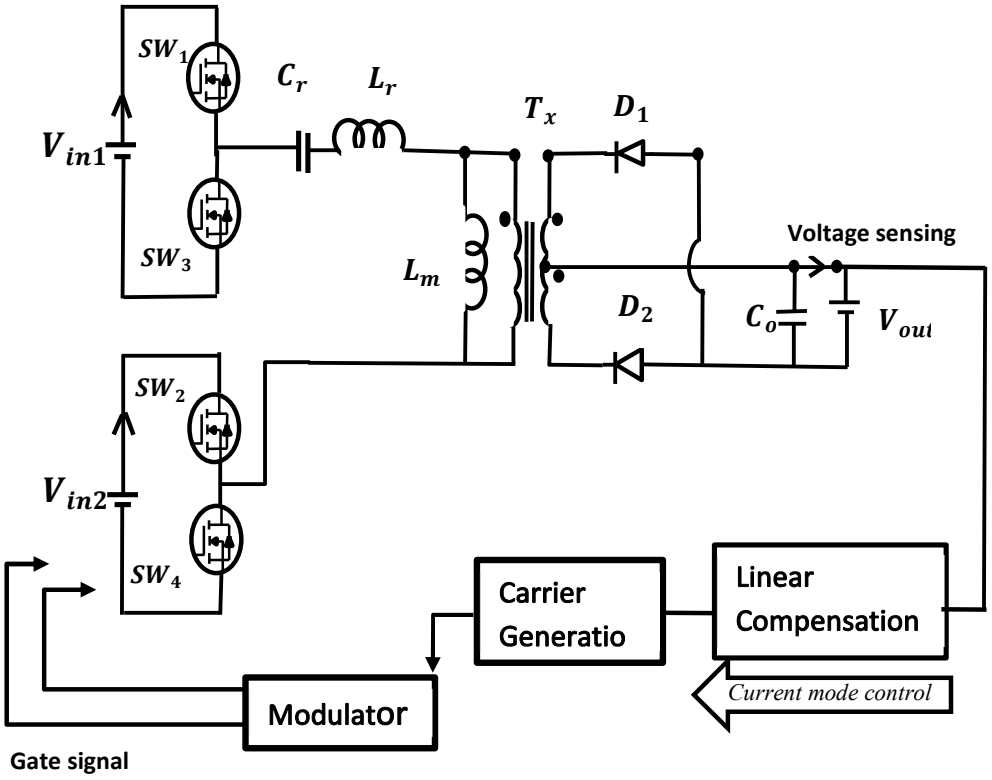

Fig.6. 5 Close loop control of DICT Resonant converter

Performance Evaluation:

The proposed topology is validated through MATLAB simulation results for dynamic charging. The Charger is shown charging Lithium-Ion battery of 72V,60Ah from two PV Panel fed 190V DC bus. The parameters of resonant tank circuit are Lr=42.3µH, Lm=136µH and Cr=26.6n which is operating closely above the resonant frequency of 150kHz. Charging of Lithium Ion Battery at three different load condition is shown in Fig.6.6. The battery is charging at full load condition at the start with subsequent load change to 50% light load and 10% light load at the end. It may be observed that no oscillation is observed at the load changes and battery smoothly settles with dynamic load changes with fast settling time of 0.7ms at full load, 0.8ms from full load to 50% loading and 2ms from 50% loading to 10% loading which validates the fast-charging capability of the proposed topology without any extra control circuitry. Fig. 6.7 depicts the state plane trajectory at full load charging. The state plane trajectory validates the stable operation of the charger along the projected trajectory. Fig.6.8(a) and Fig.6.8(b) shows gate pulse for primary side switches at 150kHz and 50% duty ratio including the dead time required for feedback diode conduction for ensuring ZVS condition. Resonant capacitor, resonant inductor and magnetizing inductor, voltage and current waveform are depicted across Fig.6.8(c) to Fig.6.8(g) depicting the successful resonant tank operation with peak voltage across resonant capacitor as twice the input voltage.

6.3 Simulation Results

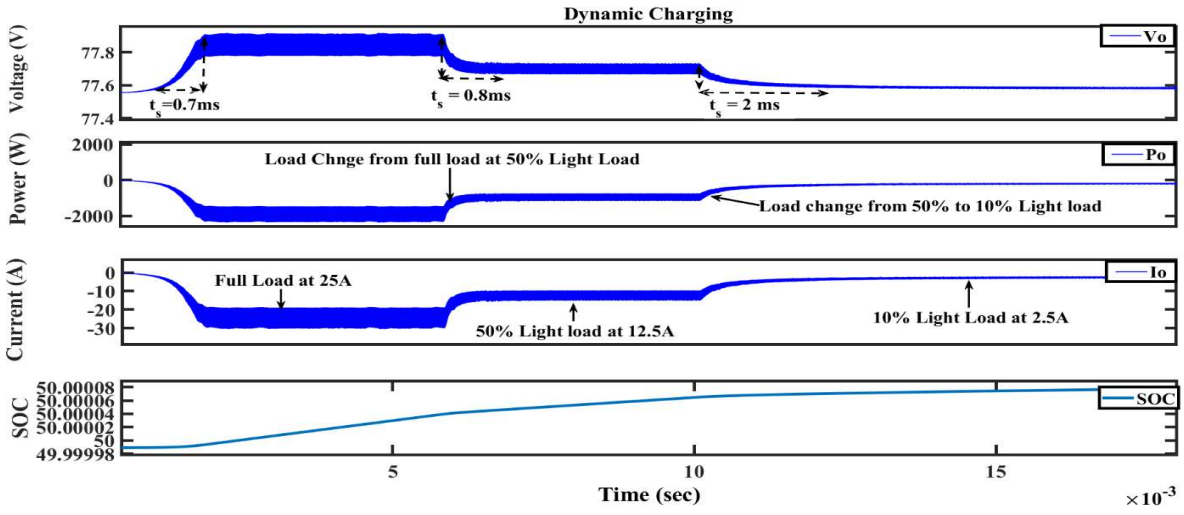

Fig.6. 6 Dynamic Charging at full load, 50% light load and 10% light load

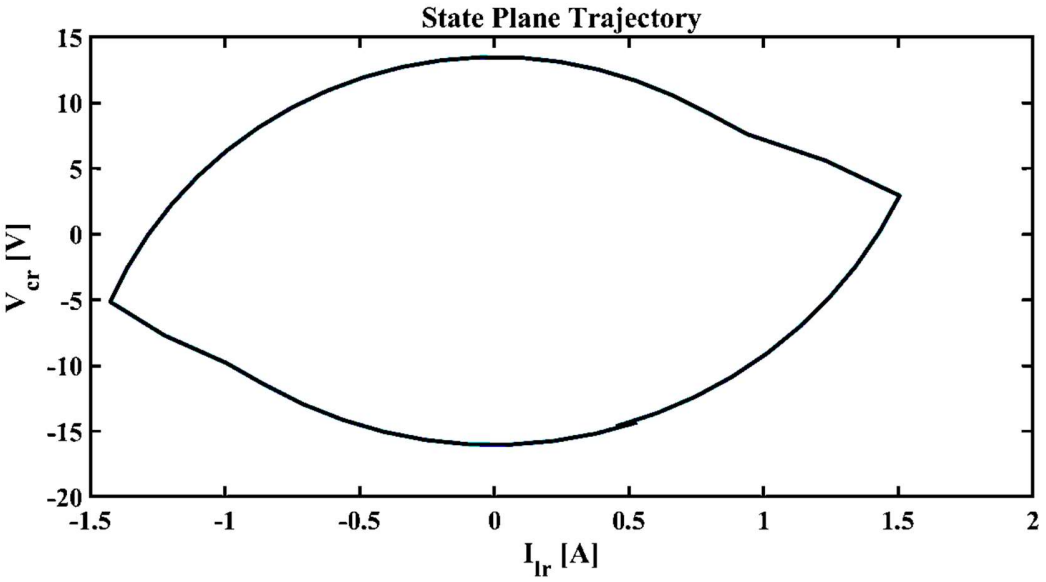

Fig.6. 7 State Pane trajectory at full load

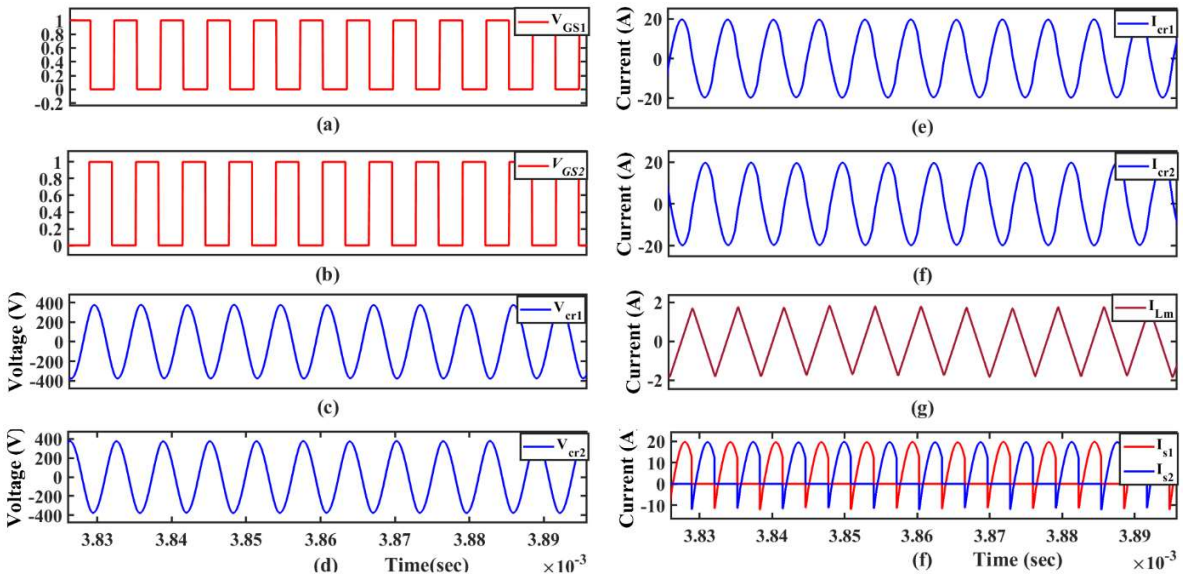

Fig.6. 8 Time domain waveform of resonant tank parameters with primary side switch gate pulses

6.4 Chapter Summary:

A new topology with dual input source and common resonant tank is investigated for off grid EV charging. Simulation study of proposed charger shows the fast-charging ability of the proposed topology with smooth transition with dynamic load changes.

CHAPTER 7
CONCLUSION

The current focus of researcher around the globe is to develop high power density converters that can effectively and efficiently do the voltage level changes to support dc distribution network. The required dc-dc converter should work on different input voltage ranges, wide output voltage level and power ranges from full load to light load (50%/10%/1%). To reduce the component size the operating switching frequency is required to kept high and soft switching is desired to ensure high efficiency.

Over the years LLC has been established as industry standard for its usage in SMPS and fast charging stations it operates with low switching losses, utilizing sinusoidal flux coupling for efficient magnetic circuit operation and exhibits operation with wider input voltage range and load perturbations.

7.1 Summary

This thesis presents the development, design and control of large step-down LLC resonant converter. The converter is designed to step down 380V DC bus to 96V DC at 3.3kW power level. Chapter 2 draws the comparison between series resonant, parallel resonant, LCC and LLC topology. The Zero voltage region (ZVS) and zero current region (ZCS) are demonstrated using gain plot at different quality factor. The different mode of operation along with the respective trajectory plot of each mode is derived. Chapter 3 focuses on comparison of different control techniques. Control algorithm with variable frequency control is utilized and effectiveness of the proposed control algorithm is demonstrated using simulation results at different load changes. In Chapter 4, converter design along with high current high frequency magnetics design is explained.

In chapter 5, a new pulse splitting control technique with hybrid control for handling transients in LLC resonant converter has been investigated. It has also been observed that the proposed scheme has a fast response to load perturbations and starting transients and is able to restrict the flow of unwarranted current in the tank circuit by swiftly splitting the pulses and controlling the width of the pulses for the safety of the switches. During steady state operation, the switching frequency smoothly transacts near resonant frequency for

achieving maximum efficiency. Simulation results of 3.3KW LLC resonant converter validates the theoretical analysis. In chapter 6, the new topology for off grid EV charging is presented. A 72V,60Ah battery is charged in constant current mode with 3.3kW charger. The simulation study validates the claimed fast charging capability.

7.2 Conclusions

The following conclusions could be drawn from this thesis:

1) LLC resonant converter is prominent solution to provide high step-down power conversion with high efficiency.
2) Foil winding-based transformer is optimal solution to handle high current along with high switching frequency.
3) Variable frequency control along with proposed pulse splitting is utilized to handle transient condition.
4) Pulse splitting control technique with hybrid control for handling transients in LLC resonant converter
5) Proposed PV fed DICT resonant converter is optimal solution for off grid EV charging.

REFEEENCES:

[1] A. T. Elsayed, A. A. Mohamed, and O. A. Mohammed, “DC microgrids and distribution systems: An overview,” *Electric Power Systems Research*, vol. 119. Elsevier Ltd, pp. 407–417, 2015. doi: 10.1016/j.epsr.2014.10.017.

[2] P. Prabhakaran, Y. Goyal, and V. Agarwal, “Novel nonlinear droop control techniques to overcome the load sharing and voltage regulation issues in DC Microgrid,” *IEEE Transactions on Power Electronics*, vol. 33, no. 5, pp. 4477–4487, May 2018, doi: 10.1109/TPEL.2017.2723045.

[3] S. J. Gunter and D. J. Perreault, “Investigation and Application of High-Efficiency Large-Step-Down Power Conversion Architectures,” 2009.

[4] J. Zeng, G. Zhang, S. S. Yu, B. Zhang, and Y. Zhang, “LLC resonant converter topologies and industrial applications -A review,” *Chinese Journal of Electrical Engineering*, vol. 6, no. 3. Institute of Electrical and Electronics Engineers Inc., pp. 73–84, Sep. 01, 2020. doi: 10.23919/CJEE.2020.000021.

[5] M. Mohammadi and M. Ordonez, “Extreme start-up response of LLC converters using average geometric control,” 2016. doi: 10.1109/ECCE.2016.7855106.

[6] M. Mohammadi and M. Ordonez, “Inrush Current Limit or Extreme Startup Response for LLC Converters Using Average Geometric Control,” *IEEE Transactions on Power Electronics*, vol. 33, no. 1, pp. 777–792, Jan. 2018, doi: 10.1109/TPEL.2017.2666803.

[7] W. Feng, F. C. Lee, and P. Mattavelli, “Simplified optimal trajectory control (SOTC) for LLC resonant converters,” *IEEE Transactions on Power Electronics*, vol. 28, no. 5, pp. 2415–2426, 2013, doi: 10.1109/TPEL.2012.2212213.

[8] W. Feng, F. C. Lee, and P. Mattavelli, “Optimal trajectory control of burst mode for LLC resonant converter,” *IEEE Transactions on Power Electronics*, vol. 28, no. 1, pp. 457–466, 2013, doi: 10.1109/TPEL.2012.2200110.

[9] C. Q. Lee and K. Siri, “Analysis and Design of Series Resonant Converter by State-Plane Diagram,” *IEEE Transactions on Aerospace and Electronic Systems*, vol. AES-22, no. 6, pp. 757–763, 1986, doi: 10.1109/TAES.1986.310811.

[10] E. X. Yang, F. C. Lee, and M. M. Jovanovic, “Small-signal modeling of LCC resonant converter,” in *PESC Record - IEEE Annual Power Electronics Specialists Conference*, 1992, pp. 941–948. doi: 10.1109/PESC.1992.254782.

[11] B. B. Malik Elsammany Elbuluk, “RESONANT CONVERTERS: TOPOLOGIES, DYNAMIC MODELING AND CONTROL,” 1976.

[12] D. Fu, F. C. Lee, M. Xu, F. Wang, W. T. Baumann, and M. Reynolds, “Topology Investigation and System Optimization of Resonant Converters,” 2010.

[13] F. Musavi, M. Craciun, D. S. Gautam, W. Eberle, and W. G. Dunford, “An LLC resonant dc-dc converter for wide output voltage range battery charging applications,” *IEEE Transactions on Power Electronics*, vol. 28, no. 12, pp. 5437–5445, 2013, doi: 10.1109/TPEL.2013.2241792.

[14] S. D. Johnson and R. W. Erickson, “STEADY-STATE ANALYSIS AND DESIGN OF THE PARALLEL RESONANT CONVERTER.,” in *PESC Record - IEEE Annual Power Electronics Specialists Conference*, 1986, pp. 154–165. doi: 10.1109/pesc.1986.7415559.

[15] E. X. Yang, B. Choi, F. C. Lee, and B. H. Cho, “Dynamic analysis and control design of LCC resonant converter,” in *PESC Record - IEEE Annual Power Electronics Specialists Conference*, 1992, pp. 362–369. doi: 10.1109/PESC.1992.254651.

[16] Y. H. Hsieh and F. C. Lee, “Small-Signal Dynamic and High-Bandwidth Design of LLC Resonant Converters,” in *ECCE 2020 - IEEE Energy Conversion Congress and Exposition*, Oct. 2020, pp. 6136–6143. doi: 10.1109/ECCE44975.2020.9235376.

[17] S. K. Pidaparthy, B. Choi, and J. Jang, “Design and performance evaluation of digital control for LLC series resonant dc-to-dc converters,” in *2014 International Power Electronics Conference, IPEC-Hiroshima - ECCE Asia 2014*, 2014, pp. 3638–3645. doi: 10.1109/IPEC.2014.6870021.

[18] Z. Hu, “TOPOLOGY, CONTROL, AND DESIGN OF LLC RESONANT CONVERTERS,” 2014.

[19] V. Panov and B. Eng, “LLC RESONANT CONVERTER MODELLING,” 2014.

[20] A. Tech-Day and H. Huang, “LLC Resonant Half Bridge Converter.”

[21] Y. Wei, Q. Luo, and H. A. Mantooth, “Synchronous Rectification for LLC Resonant Converter: An Overview,” *IEEE Transactions on Power Electronics*, vol. 36, no. 6. Institute of Electrical and Electronics Engineers Inc., pp. 7264–7280, Jun. 01, 2021. doi: 10.1109/TPEL.2020.3040603.

[22] R. Oruganti and F. C. Lee, “IA-21.”

[23] J. Deng, S. Li, S. Hu, C. C. Mi, and R. Ma, “Design methodology of LLC resonant converters for electric vehicle battery chargers,” *IEEE Transactions on Vehicular Technology*, vol. 63, no. 4, pp. 1581–1592, 2014, doi: 10.1109/TVT.2013.2287379.

[24] F. Musavi, M. Craciun, D. S. Gautam, and W. Eberle, “Control strategies for wide output voltage range LLC resonant DC-DC converters in battery chargers,” *IEEE Transactions on Vehicular Technology*, vol. 63, no. 3, pp. 1117–1125, 2014, doi: 10.1109/TVT.2013.2283158.

[25] J. Deng, C. C. Mi, R. Ma, and S. Li, “Design of LLC Resonant Converters Based on Operation-Mode Analysis for Level Two PHEV Battery Chargers,” *IEEE/ASME Transactions on Mechatronics*, vol. 20, no. 4, pp. 1595–1606, Aug. 2015, doi: 10.1109/TMECH.2014.2349791.

[26] Y. K. Lei, W. Dunford, M. Craciun, and D. Gautam, “Implementing adaptive digital control on an existing LLC DC-DC resonant converter,” Sep. 2015. doi: 10.1109/COMPEL.2015.7236484.

[27] C. Buccella, C. Cecati, H. Latafat, and K. Razi, “Digital control of a half-bridge LLC resonant converter,” 2012. doi: 10.1109/EPEPEMC.2012.6397488.

[28] W. Feng, F. C. Lee, and P. Mattavelli, “A hybrid strategy with simplified optimal trajectory control for LLC resonant converters,” in *Conference Proceedings - IEEE Applied Power Electronics Conference and Exposition - APEC*, 2012, pp. 1096–1103. doi: 10.1109/APEC.2012.6165955.

[29] S. L. Holt, C. F. Lynn, J. M. Parson, J. C. Dickens, A. A. Neuber, and J. J. Mankowski, “Burst mode operation of a high peak power high pulse repetition rate capacitor charging power supply,” in *Digest of Technical Papers-IEEE International Pulsed Power Conference*, Oct. 2015, vol. 2015-October. doi: 10.1109/PPC.2015.7297029.

[30] C. Fei, Q. Li, and F. C. Lee, “Digital implementation of light-load efficiency improvement for high-frequency LLC converters with simplified optimal trajectory control,” *IEEE Journal of Emerging and Selected Topics in Power Electronics*, vol. 6, no. 4, pp. 1850–1859, Dec. 2018, doi: 10.1109/JESTPE.2018.2832135.

[31] C. Fei, D. S. Ha, V. A. Centeno, and S. C. Southward, “Optimization of LLC Resonant Converters: State-trajectory Control and PCB based Magnetics,” 2018.

[32] F. C. Lee, Q. Li, and A. Nabih, “High Frequency Resonant Converters: An Overview on the Magnetic Design and Control Methods,” *IEEE Journal of*

Emerging and Selected Topics in Power Electronics, vol. 9, no. 1, pp. 11–23, Feb. 2021, doi: 10.1109/JESTPE.2020.3011166.

[33] A. Nabih, M. H. Ahmed, Q. Li, and F. C. Lee, "Transient Control and Soft Start-Up for 1-MHz LLC Converter with Wide Input Voltage Range Using Simplified Optimal Trajectory Control," *IEEE Journal of Emerging and Selected Topics in Power Electronics*, vol. 9, no. 1, pp. 24–37, Feb. 2021, doi: 10.1109/JESTPE.2020.2973660.

[34] Y. Wang, Z. Yan, M. Tian, and Y. Xiao, "Positive/negative pulse charging technology of battery based on PFC-LLC topology," in *Proceedings - 5th International Conference on Instrumentation and Measurement, Computer, Communication, and Control, IMCCC 2015*, Feb. 2016, pp. 1031–1036. doi: 10.1109/IMCCC.2015.223.

[35] J. Chen, C. Yang, S. Tang, and J. Zou, "A High Power Interleaved Parallel Topology Full-Bridge LLC Converter for Off-Board Charger," *IEEE Access*, vol. 9, pp. 157790–157799, 2021, doi: 10.1109/ACCESS.2021.3130051.

[36] D. Cittanti, M. Gregorio, E. Armando, and R. Bojoi, "Digital Multi-Loop Control of an LLC Resonant Converter for Electric Vehicle DC Fast Charging," in *ECCE 2020 - IEEE Energy Conversion Congress and Exposition*, Oct. 2020, pp. 4423–4430. doi: 10.1109/ECCE44975.2020.9236177.

LIST OF PUBLICATION

1. Pulse Splitting cum Width Control for Transient Handling in LLC Resonant Converter